IEEE Transactions on Robotics (T-RO) paper, presented at ICRA 2023, London, UK. Cite as T-RO paper.

An Investigation on the Effect of Actuation Pattern on the Power Consumption of Legged Robots for Extraterrestrial Exploration

Yuan Hu, Weizhong Guo, and Rongfu Lin

***Abstract*—Legged robots have great potential to be extraterrestrial exploration rovers of extraordinary versatility. Minimizing power consumption is of vital importance in the scenarios of extraterrestrial explorations. The actuation pattern, which refers to the combination of necessary actuators that output torque, has a significant influence on the power consumption of legged robots. This article seeks to investigate the effect of actuation patterns on the power consumption of legged robots that perform motion in a quasi-static manner. The power consumption model of legged robots considering actuation patterns is deduced. Based on that, the effect of the actuation pattern on mechanical power and heat power, which are the main power-loss terms, is investigated. The lowest power consumption under various conditions achieved by different actuation patterns is investigated. Simulation results show that the power consumption can be reduced by choosing the actuation pattern properly. Furthermore, the principles of selecting the optimal actuation pattern from the perspective of power consumption are summarized, which are expected to facilitate the minimal power consumption motion planning of legged robots.**

***Index Terms*—Actuation redundancy, Parallel robot, Legged robot, Motion planning, Power consumption minimization.**

I. Introduction

THE exploration of deep space has long fascinated humanity, while our knowledge about the Universe has substantially enriched by sending robots and rovers to explore celestial bodies [1], [2]. These uninhabited worlds are generally characterized by rough, harsh, and complex terrains, which proposes enormous challenges to rovers. Legged robots have great potential for extraterrestrial exploration missions owing to their remarkable maneuverability. Various concepts and prototypes have been proposed, such as the SpaceClimber [3], the SpaceBok [4], the LEMUR 3 [5], the ATHLETE [6], and the legged mobile lander [7].

The power sources used in deep space exploration missions are usually radioisotope thermoelectric generators (RTGs) or solar panels; due to their strictly restricted size and mass, either power source provides severely limited energy and power budget [8], [9]. Therefore, one key concern of space exploration is the reduction of power consumption, which is crucial to the efficiency and the lifespan of rovers.

In the literature, various measures have been incorporated to reduce the power and energy consumption of legged robots, such as using lightweight materials [10], designing high-efficiency drive system [11], and optimizing the mechanical design [12], [13]. Moreover, optimizing the motion, actuation, and control [14], [15], [16] has attracted a large amount of research interest since these approaches can exploit the potential of robots that embody state-of-the-art technology.

Robots usually move slowly in the scenario of celestial explorations. For example, the Yutu-2 rover traveled about 380m during the first 15 lunar days [17], the LEMUR 3 moved at 0.16m/hr during a rock climbing demonstration [5]. This article studies multi-legged robots that work in a quasi-static manner, which require at least three support legs to maintain equilibrium. Hence, the robot and the ground can be treated as an equivalent parallel robot by adding a *contact joint* to each support foot (a contact joint is a virtual joint that can model the relative motion between the support foot and the ground) [18]. The robot body, the ground, and the support legs are considered to be the moving platform, the base, and the limbs of the equivalent parallel robot, respectively. For a general multi-legged robot that is capable of omnidirectional static walking, each leg should have at least three-degree-of-freedom and thus three actuated joints. Therefore, the equivalent parallel robot has at least nine actuated joints, which is a redundantly actuated parallel robot (RAPR) or a redundantly actuated parallel mechanism (RAPM).

It is noteworthy that the existence of the equivalent parallel robot is based on the premise that all the contact joints represent the allowed feet motion correctly. For example, if each support foot forms a point contact with the ground, and the contact force at each foot lies in the friction cone, the legged robot and the ground can be treated as an equivalent parallel robot whose limbs are connected to the ground through spherical joints [19]. However, if the contact force is out of the friction cone or the leg pulls the foot, the spherical joint cannot model the motion of a support foot correctly, and thus the equivalent parallel robot will be nonexistent. Therefore, the contact forces need to be distributed to fulfill certain constraints. Alternatively, a legged robot can anchor all the feet on the ground firmly with properly designed mechanisms, such as the microspine tool introduced in [20], [5]. In this

This work was supported by the National Natural Science Foundation of China (Grant No. 51735009, 51905338) and by the State Key Laboratory of Mechanical System and Vibration Project (Grant No. MSVZD202008). *(Corresponding author: Weizhong Guo.)*

Y. Hu was with the State Key Laboratory of Mechanical System and Vibration, School of Mechanical Engineering, Shanghai Jiao Tong University, Shanghai 200240, China. He is now with the School of Mechanical Engineering, University of Shanghai for Science and Technology, Shanghai 200093, China (e-mail: hu_yuan_@126.com).

W. Guo and R. Lin are with the State Key Laboratory of Mechanical System and Vibration, School of Mechanical Engineering, Shanghai Jiao Tong University, Shanghai 200240, China (e-mail: wzguo@sjtu.edu.cn; rongfulin@sjtu.edu.cn).

IEEE Transactions on Robotics (T-RO) paper, presented at ICRA 2023, London, UK. Cite as T-RO paper.

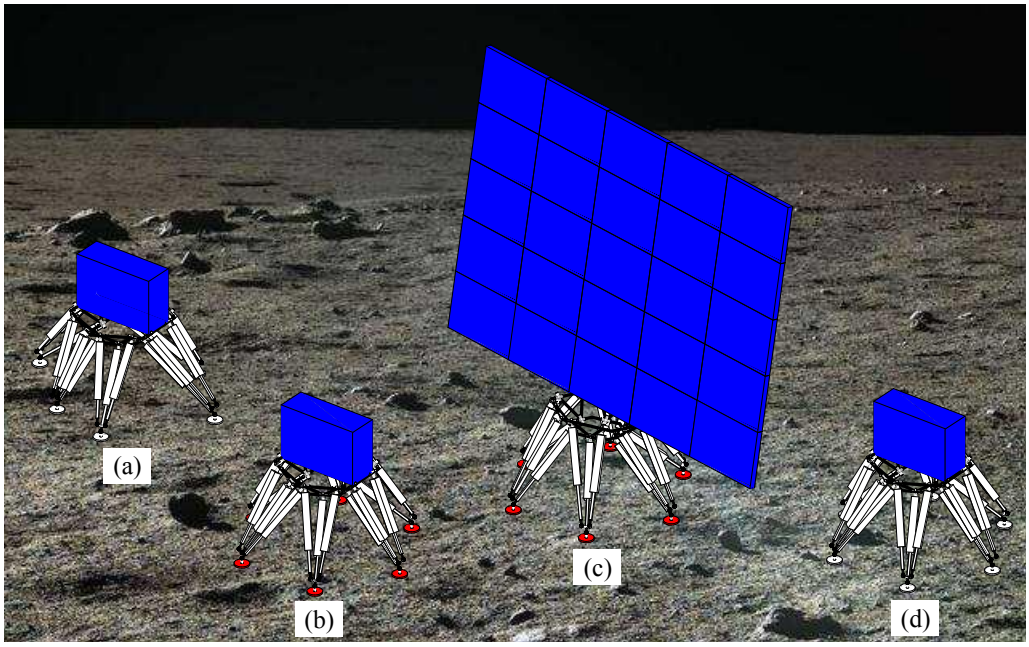

Fig. 1: Exploration mode of an extraterrestrial legged robot. (a) Travel. (b) Anchor the feet (the anchored feet are drawn in red). (c) Deploy the solar array panels. The legged robot manipulates the solar array panels to keep them towards the sun for the highest electric power generation. (d) Stow the solar array panels and release the feet.

way, the limbs of the equivalent parallel robot connect to the base through fixed connections, and thus there is no need to consider the contact force constraints (assuming the fixed connections are strong enough).

An equivalent parallel robot can perform tasks that are difficult or even impossible for a single leg of the legged robot. For example, the extraterrestrial legged robot shown in Fig. 1 can be considered to be a parallel robot after all the feet are anchored on the ground. The equivalent parallel robot can provide a much higher load-bearing capacity than each leg and thus can operate deployable solar array panels that are too heavy to be operated by a single leg.

Some studies have been performed to minimize the energy consumption of RAPMs by exploiting their actuation redundancy. A RAPM optimization procedure is proposed to minimize the energy consumption by using an optimizer to distribute torques [21]. It is proved that the energy consumption of a RAPM could be minimized by distributing actuating torques properly [22], this idea is incorporated into the design of an energy-efficient robotic leg [23]. In [23], the authors also noticed that the energy efficiency of a RAPM could be affected by the choice of actuated joints. These studies show that the power and energy consumption of a RAPM can be minimized by optimizing the actuating torques. An underlying principle of these studies is that all actuators output torques.

For an electrical motor, the magnitude of the torque is linearly related to the mechanical power, and the square of the torque is linearly related to the heat power. Therefore, an actuator consumes power when it outputs torque and no power when it follows its external motion and does not output torque (other costs are ignored). Two definitions are given below to differentiate the actuation states of an actuator:

- A *host actuator* is an actuator that outputs torque or force;
- A *slave actuator* is an actuator that follows its external motion while it outputs no torque or force.

A combination of host and slave actuators is called an *actuation pattern*, which contains two characteristics, namely the number and the specific arrangement of the host actuators. For the sake of simplicity, this article assumes that each actuated joint is driven by one actuator. A joint driven by a host actuator is called a *host joint*, and a joint driven by a slave actuator is called a *slave joint*.

Intuitively, more power is demanded if a RAPR has a larger number of host actuators. This intuitive impression indicates that the power consumption of a RAPR that has a sufficient number of actuators could be reduced by choosing a proper actuation pattern. To our best knowledge, no previous study considered the possibility of reducing the power consumption of RAPRs with this approach.

Now, a natural question is that does a legged robot's power consumption can be reduced by choosing the actuation pattern properly? If it does, how does the actuation pattern affects the power consumption? And finally, how to choose the optimal actuation pattern in the sense of power consumption? This article seeks to address these questions.

This work will facilitate the designing of motion planning methods considering the actuation pattern optimization, which is a new option to reduce the power consumption of legged robots that work in a quasi-static manner. However, the study of motion planning is beyond the scope of this article.

This article is organized as follows. Section II provides some preliminary materials necessary for the rest of this article. Section III gives the representation of actuation patterns and discusses feasible actuation patterns. Section IV deduces the

power consumption model of legged robots considering actuation patterns. Section V investigates the effect of actuation patterns on the power consumption of legged robots under various conditions. Finally, Section VI concludes this article.

II. Preliminary material

This section provides a brief introduction to the screw theory, which will be necessary for the rest of this article.

A. Screw, Reciprocal screw

A screw $\$$ is a geometric entity that can be represented as a six-vector containing five independent quantities:

$$\$ = \begin{bmatrix} \boldsymbol{s} \\ \boldsymbol{s}_0 \end{bmatrix} = \begin{bmatrix} \boldsymbol{s} \\ \boldsymbol{r} \times \boldsymbol{s} + h\boldsymbol{s} \end{bmatrix} = [l, m, n, p, q, r]^T, \quad (1)$$

where $\boldsymbol{s}$ is called the primary part which represents the axis direction vector of $\$$; $\boldsymbol{s}_0 = \boldsymbol{r} \times \boldsymbol{s} + h\boldsymbol{s}$ is called the secondary part, $\boldsymbol{r}$ is a point on the screw axis, $h = (\boldsymbol{s} \cdot \boldsymbol{s}_0) / (\boldsymbol{s} \cdot \boldsymbol{s})$ is the pitch of $\$$; $[l, m, n, p, q, r]^T$ is called the Plücker coordinates of $\$$. The Plücker coordinates can be expressed in ray order and axis order [24]. This article uses the ray order convention.

If the pitch h is zero, the screw $\$$ is called a line vector, which can be represented as follows:

$$\$ = \begin{bmatrix} \boldsymbol{s} \\ \boldsymbol{r} \times \boldsymbol{s} \end{bmatrix}. \quad (2)$$

If the pitch h is infinite, the screw $\$$ is called a couple, which can be represented as follows:

$$\$ = \begin{bmatrix} \boldsymbol{0}_{3\times1} \\ \boldsymbol{s} \end{bmatrix}. \quad (3)$$

The mutual moment of two screws $\$_1 = [l_1, m_1, n_1, p_1, q_1, r_1]^T$ and $\$_2 = [l_2, m_2, n_2, p_2, q_2, r_2]^T$ can be calculated as follows:

$$\$_1 \Delta \$_2 = l_1 p_2 + m_1 q_2 + n_1 r_2 + p_1 l_2 + q_1 m_2 + r_1 n_2, \quad (4)$$

where Δ is an elliptic polar operator [25], which interchanges the primary part and the secondary part of a screw. Δ can be expressed as follows:

$$\Delta = \begin{bmatrix} \boldsymbol{0}_{3\times3} & \boldsymbol{I}_{3\times3} \\ \boldsymbol{I}_{3\times3} & \boldsymbol{0}_{3\times3} \end{bmatrix}, \quad (5)$$

where $\boldsymbol{I}_{3\times3}$ is the 3×3 identity matrix. Two screws are reciprocal if their mutual moment is zero.

By attaching a velocity amplitude, a screw becomes a twist that represents linear and angular velocity [26]. A twist can be represented as:

$$\mathcal{V} = \begin{bmatrix} \boldsymbol{\omega} \\ \boldsymbol{v} \end{bmatrix}, \quad (6)$$

where $\boldsymbol{\omega}$ is the angular velocity, and $\boldsymbol{v}$ is the linear velocity. In particular, if $\mathcal{V}$ is a line vector, it represents an angular velocity; if $\mathcal{V}$ is a couple, it represents a linear velocity.

By attaching an intensity, a screw becomes a wrench that represents force and moment [26]. A wrench can be represented as:

$$\mathcal{F} = \begin{bmatrix} \boldsymbol{f} \\ \boldsymbol{m} \end{bmatrix}, \quad (7)$$

where $\boldsymbol{f}$ is the force, and $\boldsymbol{m}$ is the moment. In particular, if $\mathcal{F}$ is a line vector, it represents a pure force; if $\mathcal{F}$ is a couple, it represents a moment.

B. Screw system, Reciprocal screw system

A set of screws $\{\$_1, \$_2, \cdots, \$_N\}$ can span a screw system $\mathbb{S}$, which is a linear vector subspace. A basis set is a set of linearly independent screws that span $\mathbb{S}$ [27]. In this article, a screw system $\mathbb{S}$ is expressed by a matrix, as shown in Eq. 8. Each column of this matrix is a screw from the set of screws that spans $\mathbb{S}$. Note that $\mathbb{S}$ is the spanned subspace instead of the set of screws.

$$\mathbb{S} = [\$_1, \$_2, \cdots, \$_N]. \quad (8)$$

The dimension of $\mathbb{S}$ is written as $\dim(\mathbb{S})$, which can be calculated as:

$$\dim(\mathbb{S}) = \operatorname{rank}([\$_1, \$_2, \cdots, \$_N]), \quad (9)$$

where $\operatorname{rank}(\cdot)$ is used to express the rank of a matrix.

Two screw systems $\mathbb{S} = [\$_1, \$_2, \cdots, \$_N]$ and $\mathbb{S}^r = [\$_1^r, \$_2^r, \cdots, \$_M^r]$ are reciprocal if the following equation holds:

$$\mathbb{S}^T \Delta \mathbb{S}^r = \boldsymbol{0}_{N\times M}. \quad (10)$$

Moreover, $\mathbb{S}^r$ can be obtained as follows:

$$\mathbb{S}^r = \Delta \mathbb{N}\left(\mathbb{S}^T\right), \quad (11)$$

where $\mathbb{N}\left(\mathbb{S}^T\right)$ is the null space of the transpose of $\mathbb{S}$. The null space can be constructed accurately and efficiently with the method developed by Dai et al. [28]. When $\mathbb{S}$ is of full rank, $\mathbb{S}^r$ consists of the trivial solution $[0, 0, 0, 0, 0, 0]^T$, thus:

$$\dim(\mathbb{S}^r) = \operatorname{rank}(\mathbb{S}^r) = 0. \quad (12)$$

When $\mathbb{S}$ is not of full rank [28],

$$\dim(\mathbb{S}^r) = \operatorname{rank}(\mathbb{S}^r) = 6 - \operatorname{rank}(\mathbb{S}). \quad (13)$$

C. Screw systems of parallel mechanisms

The *leg motion-screw system*, the *leg constraint-screw system*, the *body motion-screw system*, and the *body constraint-screw system* are relevant to the rest of this article.

The *i*th leg motion-screw system $\mathbb{S}_{l_i}$ spans the relative motion between the moving platform and the base allowed by the *i*th leg.

The *i*th leg constraint-screw system $\mathbb{S}_{l_i}^r$ spans the constraint between the moving platform and the base generated by the *i*th leg. $\mathbb{S}_{l_i}^r$ and $\mathbb{S}_{l_i}$ are reciprocal screw systems.

The body motion-screw system $\mathbb{S}_b$ spans the possible motion between the moving platform and the base. Suppose a parallel mechanism has *p* legs, then [27]:

$$\mathbb{S}_b = \mathbb{S}_{l_1} \cap \mathbb{S}_{l_2} \cap \cdots \cap \mathbb{S}_{l_p}, \quad (14)$$

where $\cap$ denotes the intersection of screw systems.

The body constraint-screw system $\mathbb{S}_b^r$ spans the constraint between the moving platform and the base generated by all the legs. Suppose a parallel mechanism has *p* legs, then [27]:

$$\mathbb{S}_b^r = \mathbb{S}_{l_1}^r \cup \mathbb{S}_{l_2}^r \cup \cdots \cup \mathbb{S}_{l_p}^r, \quad (15)$$

where $\cup$ denotes the union of screw systems. $\mathbb{S}_b^r$ and $\mathbb{S}_b$ are reciprocal screw systems. Thus, according to Eq. 11:

$$\mathbb{S}_b = \Delta \mathbb{N}\left(\left(\mathbb{S}_b^r\right)^T\right). \quad (16)$$

III. Actuation pattern

A. Representation of actuation patterns

Suppose a legged robot has n_D actuated joints, which are labeled with $\mathrm{J}_1, \mathrm{J}_2, \cdots, \mathrm{J}_{n_D}$. Thus an arbitrary actuation pattern $\mathcal{P}$ of this robot can be represented as follows:

$$\mathcal{P} = [g(\mathrm{J}_1), g(\mathrm{J}_2), \cdots, g(\mathrm{J}_{n_D})], \tag{17}$$

where $g(\cdot)$ is a function determining logical 1 (true) or 0 (false) according to the actuation status of the joint. $g(\cdot)$ can be expressed as follows:

$$g(\mathrm{J}_i) = \begin{cases} 1 & \text{if } \mathrm{J}_i \text{ is a host joint} \\ 0 & \text{if } \mathrm{J}_i \text{ is a slave joint} \end{cases}, \ i = 1, 2, \cdots, n_D. \tag{18}$$

Note that all the joints in swing legs should always be host joints during the swing motion since there is no external force acting on the feet to help these legs move. Therefore, only the actuation status of actuated joints in the support legs can be adjusted. However, the actuation status of swing legs' actuated joints is also represented in Eq. 17. Thus, this equation can be applied to different walking phrases, which are associated with different combinations of support legs and swing legs.

Unless otherwise stated, the rest of this article refers to host actuators, host joints, slave actuators, and slave joints in the support legs as host actuators, host joints, slave actuators, and slave joints, respectively.

B. Feasible actuation patterns

1) The definition of the feasible actuation pattern: In this article, an actuation pattern that enables a legged robot to possess the demanded motion is called a *feasible actuation pattern*. More specifically, a feasible actuation pattern should enable the legged robot to possess the demanded posture (the *posture* of a kinematic chain refers to the pose of all the linkages of the kinematic chain [29]), velocity, and acceleration. For a legged robot that works in a quasi-static manner, a feasible actuation pattern should be able to enable it to keep stationary at the demanded posture.

2) The criterion to select the feasible actuation pattern: As mentioned before, a legged robot and the ground can be considered to be an equivalent parallel robot by adding a contact joint to each support foot. For simplicity, suppose the legged robot's legs are not kinematically redundant mechanisms and are with non-singular configurations. Under these assumptions, if the equivalent parallel robot can keep stationary, its body can keep stationary, and vice versa. Therefore, the rank of the body motion-screw system corresponding to a feasible actuation pattern should be zero, and according to Eq. 13, the corresponding body constraint-screw system's rank should be six. Therefore, it is necessary to analyze the body constraint-screw system to select the feasible actuation pattern.

Without loss of generality, suppose a legged robot's support legs are $leg_1, leg_2, \cdots, leg_k$, as shown in Fig. 2. The corresponding contact joints are $\mathrm{J}_1^C, \mathrm{J}_2^C, \cdots, \mathrm{J}_k^C$, the corresponding contact joint motion-screw systems are $\mathbb{S}_{\mathrm{J}_1^C}, \mathbb{S}_{\mathrm{J}_2^C}, \cdots, \mathbb{S}_{\mathrm{J}_k^C}$.

The constraints imposed on the body by a support leg are generated by the leg mechanism and the associated

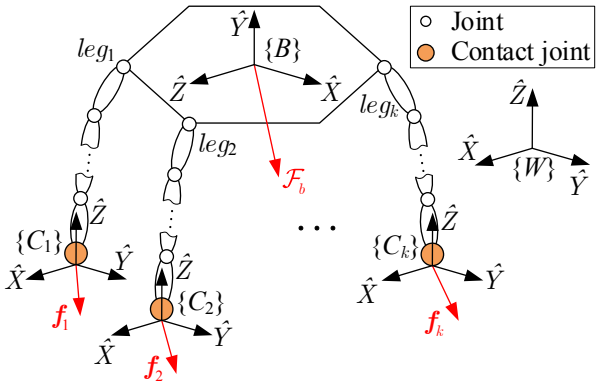

Fig. 2: A general legged robot. At this instant, there are k support legs that are $leg_1, leg_2, \cdots, leg_k$. $\boldsymbol{f}_1, \boldsymbol{f}_2, \cdots, \boldsymbol{f}_k$ are the feet contact forces. $\mathcal{F}_b$ is the resultant external wrench acting on the body. $\{C_1\}, \{C_2\}, \cdots, \{C_k\}$ are the contact frames. $\{B\}$ is the body frame. $\{W\}$ is the world frame.

contact joint. Since each support leg serially connects with the corresponding contact joint, the leg motion-screw system considering the contact joint can be deduced as follows:

$$\mathbb{S}_{l_i, \mathrm{J}_i^C} = \mathbb{S}_{l_i} \cup \mathbb{S}_{\mathrm{J}_i^C}, \ i = 1, 2, \cdots, k, \tag{19}$$

where $\mathbb{S}_{l_i}$ is the leg motion-screw system of leg_i considering the leg mechanism. Note that actuation patterns affect $\mathbb{S}_{l_i}$. The leg constraint-screw system $\mathbb{S}^r_{l_i, \mathrm{J}_i^C}$ corresponding to $\mathbb{S}_{l_i, \mathrm{J}_i^C}$ can be obtained through Eq. 11:

$$\mathbb{S}^r_{l_i, \mathrm{J}_i^C} = \Delta\mathbb{N}\left(\mathbb{S}^T_{l_i, \mathrm{J}_i^C}\right). \tag{20}$$

Now the body constraint-screw system $\mathbb{S}^r_b$ can be obtained through Eq. 15 as follows:

$$\mathbb{S}^r_b = \bigcup_{i=1}^{k} \mathbb{S}^r_{l_i, \mathrm{J}_i^C}. \tag{21}$$

For an arbitrary actuation pattern $\mathcal{P}$, if the $\mathbb{S}^r_b$ obtained above is of full rank, i.e., the relation shown in Eq. 22 exists, $\mathcal{P}$ is feasible. Otherwise, $\mathcal{P}$ is unfeasible.

$$\mathrm{rank}(\mathbb{S}^r_b) \equiv 6. \tag{22}$$

3) Determining the feasible actuation patterns: All the possible actuation patterns can be obtained by enumerating the combinations of host joints with a given host joint number n_h. Subsequently, all the feasible actuation patterns can be determined based on Eqs. 19-22.

The host joint number n_h corresponding to a possible actuation pattern is an integer between its maximum value n_{max} and minimal value n_{min}. n_{max} equals n_d, which is the total number of actuated joints in the support legs. A legged robot that can perform omnidirectional static walking should be able to translate the foot tip in three-dimensional space. Moreover, legged robots designed to work on complex terrains are typically capable of adjusting the three-dimensional orientation of the body. Thus, the robot body is capable of performing six-dimensional motion, which means the equivalent parallel robot is of six-degree-of-freedom. Therefore, the support legs

need at least six host joints to enable the legged robot to keep stationary, i.e., the minimal host joint number n_{min} is six.

By choosing n_h joints from all the n_d actuated joints in the support legs at a time, all possible actuation patterns can be obtained. The number of the possible actuation patterns that engage n_h host joints is:

$$n_{\mathcal{P}} = \frac{n_{max}!}{n_h! \cdot (n_{max} - n_h)!},\ n_{min} \leqslant n_h \leqslant n_{max}. \tag{23}$$

Note the feasibility of an actuation pattern ${}^{n_h}\mathcal{P}_i, i = 1, \cdots, n_{\mathcal{P}}$ needs to be assessed (the superscript indicates the host joint number in this actuation pattern). With a given configuration $\mathcal{C}$ of the robot, the feasibility of ${}^{n_h}\mathcal{P}_i$ at $\mathcal{C}$ can be assessed by using Eqs. 19-22. By assessing the feasibility of each and every ${}^{n_h}\mathcal{P}_i$, all the feasible actuation patterns ${}^{n_h}\mathcal{P}^f_j, j = 1, \cdots, n_{\mathcal{P}f}$ can be determined (the superscript 'f' indicates a feasible actuation pattern). Note the total number of feasible actuation patterns $n_{\mathcal{P}f}$ may vary when a different $\mathcal{C}$ or a different n_h is considered. The flowchart to determine all the feasible actuation patterns that have n_h host joints at a configuration $\mathcal{C}$ is shown in Fig. 3.

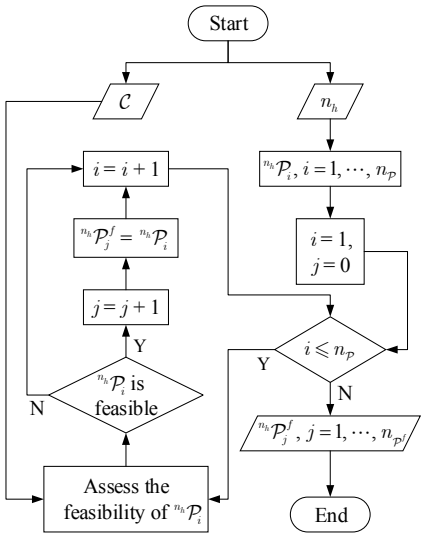

Fig. 3: Flowchart to determine the feasible actuation patterns.

IV. The power consumption model of legged robots considering actuation patterns

A. The power consumption model

The power consumption of a legged robot is the sum of the power consumed by all the actuators. Since the actuators in swing legs should always be host actuators, the power consumption of legged robots cannot be changed by adjusting the actuation status of these actuators. Moreover, the actuators in swing legs only need to counterbalance the gravity of these legs, while the actuators in support legs need to bear the gravity of the entire robot, and thus the latter are responsible for the majority part of the total power consumption. Hence, the sum of the power consumed by the actuators in supported legs is considered to be the power consumption of the legged robot. Thus,

$$P_r = \sum_{i=j_1}^{j_{n_d}} P_{m_i},\ 1 \leqslant j_1, j_2, \cdots, j_{n_d} \leqslant n_D, \tag{24}$$

where P_r is the power consumption of the robot, n_d is the total number of actuators in the support legs, P_{m_i} is the power consumed by the ith actuator of the robot.

The power consumption of an actuator or DC motor can be calculated by Eq. 25 [30], [31]. To keep the notation uncluttered, the subscripts that indicate the serial number of the actuators are ignored.

$$P_m = \delta\left(\tau_g \cdot \dot{\theta}_g\right) + \frac{R_w}{k_t^2 G^2} \cdot \tau_g^2, \tag{25}$$

where τ_g is the output torque of the gearbox, $\dot{\theta}_g$ is the output angular speed of the gearbox, R_w is the resistance of the windings, k_t is the torque constant, G is the gear ratio. When the product $\tau_g \cdot \dot{\theta}_g$ is negative, the external forces supply mechanical power to the motor. However, instead of storing this energy, DC motors consume it like dampers [30]. Therefore, the electrical power consumed by a motor due to mechanical power can be calculated by:

$$\delta\left(\tau_g \cdot \dot{\theta}_g\right) = \begin{cases} \tau_g \cdot \dot{\theta}_g & \text{if } \tau_g \cdot \dot{\theta}_g > 0 \\ 0 & \text{if } \tau_g \cdot \dot{\theta}_g \leqslant 0 \end{cases}. \tag{26}$$

For a linear actuator, the τ_g and $\dot{\theta}_g$ in Eqs. 25 and 26 represent the linear output force and the linear output speed, respectively. As mentioned before, each actuated joint is assumed to be driven by one actuator in this article. Thus, τ_g and $\dot{\theta}_g$ in Eqs. 25 and 26 equal to the joint force and joint velocity of the host joint, respectively.

According to Eq. 25, a host actuator consumes power since it outputs torque or force, whereas a slave actuator has zero power consumption because it does not output any torque or force. Therefore, Eq. 24 is equal to the following equation:

$$P_r = \sum_{k=i_1}^{i_{n_h}} P_{m_k}, \{i_1, i_2, \cdots, i_{n_h}\} \subseteq \{j_1, j_2, \cdots, j_{n_d}\}, \tag{27}$$

where $j_1, j_2, \cdots, j_{n_d}$ are the same subscripts as that in Eq. 24, P_{m_k} is the power consumed by a host actuator.

The rest of this section addresses the problem of calculating the host joint velocity vector $\dot{\boldsymbol{\theta}}_h$ and the host joint force vector $\boldsymbol{\tau}_h$, which are required to calculate the power consumption of a legged robot according to Eqs. 25-27.

B. Host joint velocity

For a legged robot that has n_d actuated joints in the support legs, the velocity kinematic model (VKM), which governs how the body twist maps to the actuated joint velocity vector of the support legs, can be expressed as:

$$\dot{\boldsymbol{\theta}}_r = J_r \cdot \mathcal{V}_b, \tag{28}$$

where $\mathcal{V}_b$ is the twist of $\{B\}$; J_r is the velocity Jacobian of the equivalent parallel robot, which has the following form:

$$J_r = \begin{bmatrix} J_{j_1} \\ J_{j_2} \\ \vdots \\ J_{j_{n_d}} \end{bmatrix}, \ 1 \leqslant j_1, j_2, \cdots, j_{n_d} \leqslant n_D, \tag{29}$$

where $J_{j_1}, J_{j_2}, \cdots, J_{j_{n_d}}$ are 1×6 vectors, each of them maps $\mathcal{V}_b$ to one actuated joint velocity; $\dot{\boldsymbol{\theta}}_r = \begin{bmatrix} \dot{\theta}_{j_1}, \dot{\theta}_{j_2}, \cdots, \dot{\theta}_{j_{n_d}} \end{bmatrix}^T$ is an $n_d \times 1$ vector which represents the actuated joint velocity vector of the support legs.

The host joint velocity vector $\dot{\boldsymbol{\theta}}_h = \begin{bmatrix} \dot{\theta}_{i_1}, \dot{\theta}_{i_2}, \cdots, \dot{\theta}_{i_{n_h}} \end{bmatrix}^T$ can be calculated as follows:

$$\dot{\boldsymbol{\theta}}_h = J_h \cdot \mathcal{V}_b, \tag{30}$$

where J_h is the velocity Jacobian corresponding to all the host joints in the support legs. J_h can be extracted from J_r as:

$$J_h = \begin{bmatrix} J_{i_1} \\ J_{i_2} \\ \vdots \\ J_{i_{n_h}} \end{bmatrix}, \{i_1, i_2, \cdots, i_{n_h}\} \subseteq \{j_1, j_2, \cdots, j_{n_d}\}, \tag{31}$$

where $J_{i_1}, J_{i_2}, \cdots, J_{i_{n_h}}$ are rows of J_r.

Note that $\dot{\boldsymbol{\theta}}_h$ can also be extracted from $\dot{\boldsymbol{\theta}}_r$, this method is faster than using Eq. 30.

C. Host joint force

This section calculates the host joint force vector of legged robots that work in a quasi-static manner. In this working status, the operational speed is slow, and the dynamic effect is negligible. The conditions that the support feet are anchored and unanchored are considered separately.

1) Anchored feet condition: Based on the premises that a legged robot works in a quasi-static manner and the feet are anchored, the joint force vector of the host joints can be calculated by the following equation, which is derived through the principle of virtual work by using Eq. 30:

$$\boldsymbol{\tau}_h = (J_h^T)^+ \cdot \mathcal{F}_b, \tag{32}$$

where $\boldsymbol{\tau}_h$ is the joint force vector of host joints, $(J_h^T)^+$ is the pseudo-inverse of the transpose of J_h, $\mathcal{F}_b$ is the resultant external wrench acting on the robot body.

The $\boldsymbol{\tau}_h$ yielded by Eq. 32 falls into one of two categories [30]:

- When the number of host actuators is 6, $(J_h^T)^+$ equals to $(J_h^T)^{-1}$, and $\boldsymbol{\tau}_h$ is the unique solution that exactly satisfies $J_h^T \cdot \boldsymbol{\tau} = \mathcal{F}_b$.
- When the number of host actuators is larger than 6, there exists an infinite number of solutions $\boldsymbol{\tau}$ to $J_h^T \cdot \boldsymbol{\tau} = \mathcal{F}_b$. However, $\boldsymbol{\tau}_h$ has the minimal two-norm among all solutions. That is, for any $\boldsymbol{\tau}$ exactly satisfying $J_h^T \cdot \boldsymbol{\tau} = \mathcal{F}_b$, $\|\boldsymbol{\tau}_h\| \leqslant \|\boldsymbol{\tau}\|$.

Thus, Eq. 32 can obtain the solution with the minimal two-norm, which is a suitable solution for minimizing the required actuator energy if there is no other limitations [32].

2) Unanchored feet condition: The host joint force vector of a legged robot can be extracted from the actuated joint force vector. The latter can be obtained with the contact wrenches at the support feet. Moreover, the contact force constraints should be considered under the condition that the feet are unanchored.

The actuated joint velocity vector $\dot{\boldsymbol{\theta}}_l$ of a leg and the corresponding foot twist $\mathcal{V}_f$ has the following relation:

$$\mathcal{V}_f = J_l \dot{\boldsymbol{\theta}}_l, \tag{33}$$

where J_l is the leg velocity Jacobian. Based on Eq. 33, the relation between the actuated joint force vector $\boldsymbol{\tau}_l$ and the generated contact wrench $\mathcal{F}_f$ can be deduced through the principle of virtual work as follows:

$$\boldsymbol{\tau}_l = J_l^T \mathcal{F}_f. \tag{34}$$

Suppose a legged robot has n legs, which are labeled with $leg_1, leg_2, \cdots, leg_n$. Suppose the support legs are $leg_1, leg_2, \cdots, leg_k$, and the corresponding actuated joint force vectors are $\boldsymbol{\tau}_{l_1}, \boldsymbol{\tau}_{l_2}, \cdots, \boldsymbol{\tau}_{l_k}$, then the actuated joint force vector of all the support legs can be expressed as follows:

$$\boldsymbol{\tau}_d = \begin{bmatrix} \boldsymbol{\tau}_{l_1} \\ \boldsymbol{\tau}_{l_2} \\ \vdots \\ \boldsymbol{\tau}_{l_k} \end{bmatrix}. \tag{35}$$

The host joint force vector $\boldsymbol{\tau}_h$ can be obtained as follows:

$$\begin{bmatrix} \boldsymbol{\tau}_h \\ \mathbf{0} \end{bmatrix} = \text{diag}\,(\mathcal{P}) \cdot \begin{bmatrix} \boldsymbol{\tau}_d \\ \mathbf{0} \end{bmatrix}, \tag{36}$$

where $\text{diag}\,(\mathcal{P})$ is a diagonal matrix with the elements of an actuation pattern $\mathcal{P}$ on the main diagonal. In Eq. 36, a zero vector is connected with $\boldsymbol{\tau}_d$; thus, the obtained vector can match the dimension of $\text{diag}\,(\mathcal{P})$. Note that the zero vector is not the actuated joint force vector of the swing legs. It is only used to facilitate the expression of the calculation. Moreover, the reason that $\boldsymbol{\tau}_d$ and the zero vector can be arranged end to end is that the group of support legs and the group of swing legs are separated from each other according to the assumption made above, i.e., the first k legs are support legs, and the last $(n-k)$ legs are swing legs. Otherwise, a number of zero elements need to be distributed among the elements of $\boldsymbol{\tau}_d$ to form a vector that can match the dimension of $\text{diag}\,(\mathcal{P})$. The assumption mentioned above is used to simplify the expression of Eq. 36. However, the above calculation procedure can be applied to any combination of support legs and swing legs.

According to Eqs. 34, 35, and 36, the contact wrenches at the support feet are required for the calculation of $\boldsymbol{\tau}_h$. Since the equivalent parallel robot corresponding to a legged robot is a RAPR, the solution of the contact wrenches is not unique. The contact wrench distribution problem can usually be solved through optimization methods [33], [34].

Assume all the contact wrenches are pure forces. This assumption is valid for legged robots that have ball-shaped feet. Fig. 2 shows a general legged robot that has ball-shaped feet. At the instant shown in Fig. 2, the legged robot has k support legs that are $leg_1, leg_2, \cdots, leg_k$, the corresponding contact forces are $\boldsymbol{f}_1, \boldsymbol{f}_2, \cdots, \boldsymbol{f}_k$, and the resultant external

wrench acting on the body is $\mathcal{F}_b$. The equilibrium equation of the legged robot can be expressed as follows [35]:

$$G \cdot \mathbf{f} = \mathcal{F}_b, \tag{37}$$

where $\mathbf{f}$ can be expressed as follows:

$$\mathbf{f} = \begin{bmatrix} \boldsymbol{f}_1 \\ \boldsymbol{f}_2 \\ \vdots \\ \boldsymbol{f}_k \end{bmatrix}. \tag{38}$$

G is the following coefficient matrix:

$$G = \begin{bmatrix} \boldsymbol{I}_{3\times3} & \boldsymbol{I}_{3\times3} & \cdots & \boldsymbol{I}_{3\times3} \\ [\boldsymbol{p}_1] & [\boldsymbol{p}_2] & \cdots & [\boldsymbol{p}_k] \end{bmatrix}, \tag{39}$$

where $[\boldsymbol{p}_1], [\boldsymbol{p}_2], \cdots, [\boldsymbol{p}_k]$ are the support feet positions expressed in the skew-symmetric form. The $[\boldsymbol{p}]$ corresponding to a point $\boldsymbol{p} = [p_x, p_y, p_z]^T$ can be expressed as follows:

$$[\boldsymbol{p}] = \begin{bmatrix} 0 & -p_z & p_y \\ p_z & 0 & -p_x \\ -p_y & p_x & 0 \end{bmatrix}. \tag{40}$$

G, $\mathbf{f}$, and $\mathcal{F}_b$ should be represented in the same frame.

In addition to the equilibrium equation, the contact forces at the support feet are subject to the constraint that the ground cannot pull the unanchored feet. Moreover, if slips need to be avoided, the tangential contact forces should be limited. This article assumes the contact feet should not slip on the ground. To express the constraints mentioned above, a contact frame $\{C_i\},\ i = 1, 2, \cdots, k$ is attached to each contact point. The $\hat{Z}$-axis of a contact frame is perpendicular to the corresponding contact tangent plane and points to the associated foot. The contact force at each support foot can be expressed in the corresponding contact frame as follows:

$${}^{C_i}\boldsymbol{f}_i = \left[{}^{C_i}f_{ix},\ {}^{C_i}f_{iy},\ {}^{C_i}f_{iz}\right]^T,\ i = 1, 2, \cdots, k. \tag{41}$$

The constraints mentioned above can be expressed as follows:

$${}^{C_i}f_{iz} \leqslant 0,\ i = 1, \cdots, k; \tag{42}$$

$$\sqrt{{}^{C_i}f_{ix}^2 + {}^{C_i}f_{iy}^2} \leqslant \mu \cdot \left|{}^{C_i}f_{iz}\right|,\ i = 1, \cdots, k, \tag{43}$$

where μ is the static coefficient of friction.

According to the definition, slave joints do not output torques or forces. More specifically, the slave joint forces obtained by Eq. 34 should be zero. Therefore, the following constraint should be considered during the force distribution:

$$\boldsymbol{\tau}_s = \text{diag}\left(\text{NOT}\left(\mathcal{P}\right)\right) \cdot \begin{bmatrix} \boldsymbol{\tau}_d \\ \mathbf{0} \end{bmatrix} = \mathbf{0}, \tag{44}$$

where $\boldsymbol{\tau}_s$ is the slave joint force vector, $\text{NOT}\left(\cdot\right)$ is the logical negation function.

In the literature, two approaches are utilized to solve the contact force distribution problem, i.e., minimization of norm of feet forces and minimization of norm of joint torques [36]. The latter can provide more energy-efficient solutions in comparison with the former [36]. Hence, the object function for the contact force distribution is chosen as follows:

$$\min\left(\|\boldsymbol{\tau}_h\|\right). \tag{45}$$

The pseudo-inverse solution of Eq. 37 does not necessarily satisfy the constraints listed in Eqs. 42, 43, and 44. Nevertheless, since the pseudo-inverse solution consists only of the forces required to maintain equilibrium and does not contain interaction force components [35], it is an appropriate initial solution to the contact force distribution problem. Thus, the initial solution can be expressed as:

$$\mathbf{f}_0 = G^+ \cdot \mathcal{F}_b, \tag{46}$$

where G^+ is the pseudo-inverse of the coefficient matrix G.

In conclusion, the contact force distribution problem considering actuation patterns can be solved as the following optimization problem:

$$\begin{cases} \text{Minimize:} & \|\boldsymbol{\tau}_h\|; \\ \text{Subject to:} & \begin{cases} G \cdot \mathbf{f} = \mathcal{F}_b, \\ {}^{C_i}f_{iz} \leqslant 0, \\ \sqrt{{}^{C_i}f_{ix}^2 + {}^{C_i}f_{iy}^2} \leqslant \mu \cdot \left|{}^{C_i}f_{iz}\right|, \\ \text{diag}\left(\text{NOT}\left(\mathcal{P}\right)\right) \cdot \boldsymbol{\tau}_d = \mathbf{0}; \end{cases} \\ \text{Initial solution:} & \mathbf{f}_0 = G^+ \cdot \mathcal{F}_b. \end{cases} \tag{47}$$

The above optimization problem can be solved with off-the-shelf software packages. The genetic algorithm solver in the Global Optimization Toolbox provided by MATLAB is utilized in this study.

After solving the contact force distribution problem, the host joint force vector under the unanchored feet condition can be obtained by using Eqs. 34, 35, and 36.

V. Effect of Actuation Pattern on Power Consumption

Since minimizing power consumption is of interest for extraterrestrial legged robots, this section investigates how the lowest power consumption of legged robots changes with the actuation pattern. First, Section V-A defines several indexes to measure the power consumption of legged robots. Second, in Sections V-B and V-C, the effect of actuation patterns on the power consumption of the hexapod robot with parallel legs is investigated by using the defined indexes. Third, Section V-D carries out numerical experiments to check whether the effect of actuation patterns on the power consumption of legged robots maintains unchanged under general conditions.

A. Indexes to measure the power consumption

The normalized power consumption (NPC), the lowest normalized power consumption (LNPC), and the mean lowest normalized power consumption (MLNPC) are defined in this section.

Based on Eqs. 25 and 27, the power consumption P_r of a legged robot is determined by the host joint velocity vector $\dot{\boldsymbol{\theta}}_h$ and the host joint force vector $\boldsymbol{\tau}_h$. Moreover, according to Sections IV-B and IV-C, $\dot{\boldsymbol{\theta}}_h$ and $\boldsymbol{\tau}_h$ are affected by the body twist $\mathcal{V}_b$ and the resultant external wrench $\mathcal{F}_b$, respectively.

In this study, the gravity of the robot body and the payload on it is considered, and no other external torque is imposed on the robot. In other words, the force component $\boldsymbol{f}_b$ of $\mathcal{F}_b$

represents the gravity force, and the torque component $\boldsymbol{m}_b$ of $\mathcal{F}_b$ represents the torque created by $\boldsymbol{f}_b$.

The NPC is the index obtained by normalizing the power consumption with the magnitude of $\boldsymbol{f}_b$ and the magnitude of $\mathcal{V}_b$, which can be defined as follows:

$$\text{NPC} = \begin{cases} P_r/(\|\boldsymbol{v}_b\| \cdot \|\boldsymbol{f}_b\|) & \text{if } \|\boldsymbol{\omega}_b\| = 0 \\ P_r/(\|\boldsymbol{\omega}_b\| \cdot \|\boldsymbol{f}_b\|) & \text{if } \|\boldsymbol{\omega}_b\| \neq 0 \end{cases}, \tag{48}$$

where $\boldsymbol{\omega}_b$ and $\boldsymbol{v}_b$ are the angular velocity and the linear velocity associated with $\mathcal{V}_b$, respectively.

The NPC defined above represents the power consumed to move a unit weight at a specific configuration $\mathcal{C}$ with the normalized $\mathcal{V}_b$. For translations, the unit of NPC is $W \cdot N^{-1} \cdot (m/s)^{-1}$. For motion that has rotation components, the unit of NPC is $W \cdot N^{-1} \cdot (rad/s)^{-1}$. Fig. 4 shows the flowchart to calculated the NPC under the anchored feet condition. Fig. 5 shows the flowchart to calculate the NPC under the unanchored feet condition. According to these flowcharts, if the $\mathcal{V}_b$ and the $\boldsymbol{f}_b$ are given, the NPC is determined by the configuration $\mathcal{C}$ and the actuation pattern $\mathcal{P}$.

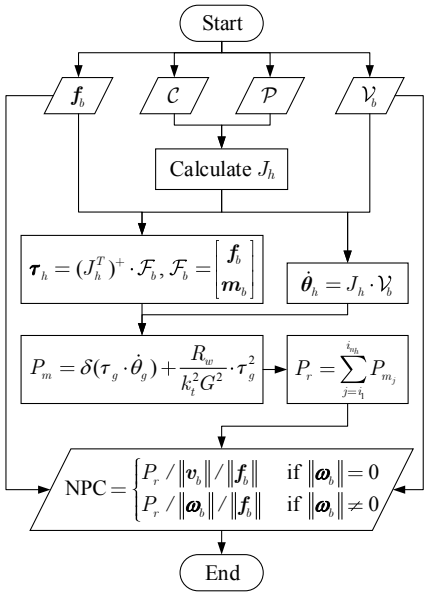

Fig. 4: Flowchart to calculate NPC under the anchored feet condition.

The LNPC is defined as the lowest NPC among all the NPC corresponding to all the feasible actuation patterns ${}^{n_h}\mathcal{P}_j^f, j = 1, \cdots, n_{\mathcal{P}^f}$ that have the same host actuator number. The actuation pattern corresponding to the LNPC is called the *optimal actuation pattern* in this article, which is represented by ${}^{n_h}_{\mathcal{C}}\mathcal{P}_{opt}$, where the subscript '$\mathcal{C}$' indicates the related configuration and the superscript 'n_h' indicates the considered host actuator number. Fig. 6 shows the flowchart to calculate LNPC. According to this flowchart, if the $\mathcal{V}_b$ and the $\boldsymbol{f}_b$ are given, the LNPC and the optimal actuator pattern ${}^{n_h}_{\mathcal{C}}\mathcal{P}_{opt}$ are determined by the configuration $\mathcal{C}$ and the host actuator number n_h.

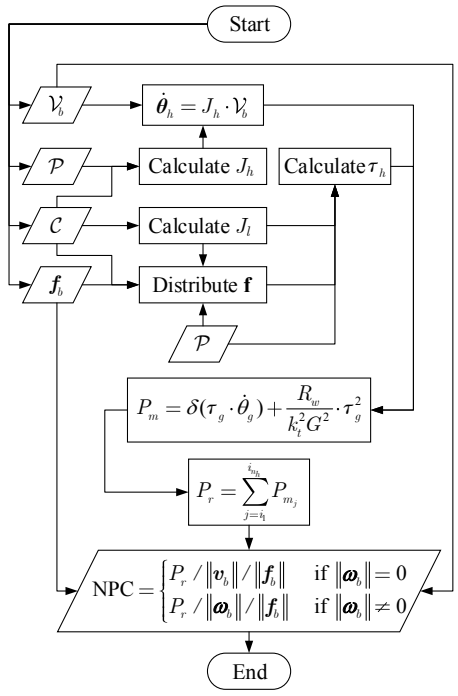

Fig. 5: Flowchart to calculate NPC under the unanchored feet condition.

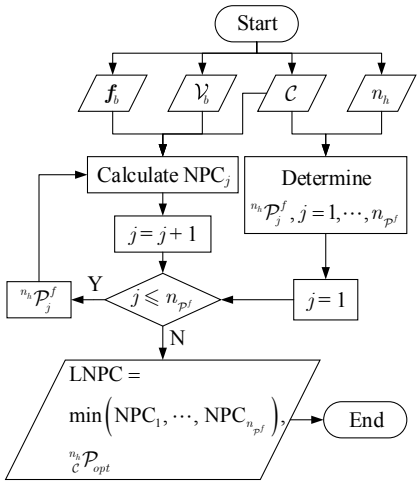

Fig. 6: Flowchart to calculate the LNPC.

The MLNPC is defined as the average value of all the LNPC that corresponding to the same host actuator number n_h in the workspace of a legged robot. For the calculation of the MLNPC, the workspace can be represented by a set of configurations $\mathcal{C}_i, i = 1, \cdots, n_{\mathcal{C}}$. The calculation flowchart of the MLNPC is shown in Fig. 7. According to this flowchart, if the $\mathcal{V}_b$ and the $\boldsymbol{f}_b$ are given, the MLNPC over the same workspace is determined by the host actuator number n_h.

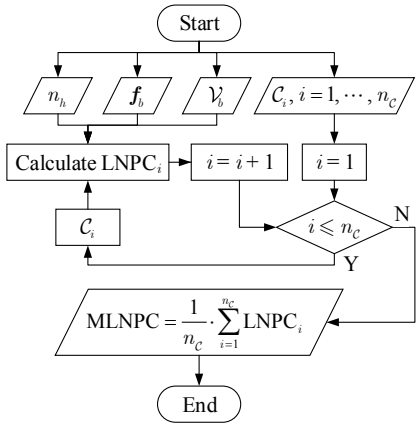

Fig. 7: Flowchart to calculate the MLNPC.

B. Effect of the actuation pattern on the lowest power consumption of the hexapod robot with parallel legs

This section investigates how the lowest power consumption of the hexapod robot with parallel legs changes with the actuation pattern. The following briefly introduces the hexapod robot, followed by the simulations.

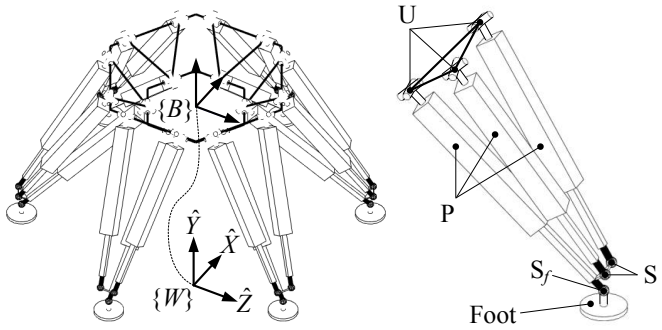

Fig. 8: Structure of the hexapod robot with parallel legs.

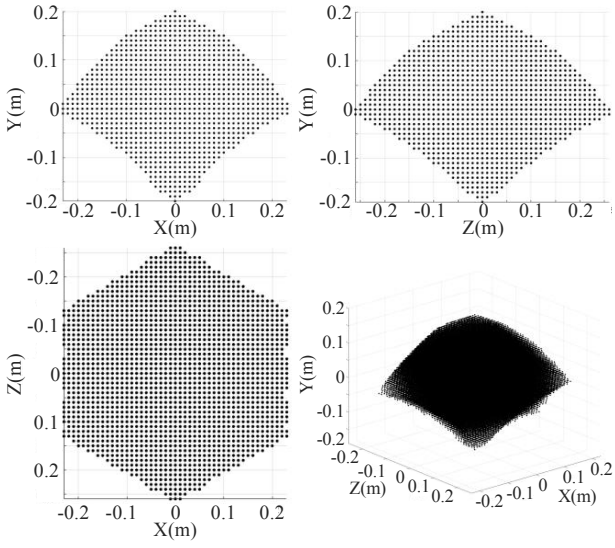

Fig. 9: Workspace of the hexapod robot with parallel legs.

The hexapod robot with parallel legs is shown in Fig. 8. This robot has six identical legs; each of them is constructed by connecting a three-degree-of-freedom parallel mechanism and a passive spherical joint (labeled as S_f) in series. The parallel mechanism consists of one UP (universal joint - prismatic joint) chain and two UPS (universal joint - prismatic joint - spherical joint) chains. The P joints in each leg are actuated, and the joint S_f allows the feet to adapt to the ground. Adhesive mechanisms, which are not depicted in Fig. 8, can be mounted on the feet, by which the feet can be anchored to the ground firmly. $\{B\}$ is the body frame, $\{W\}$ is the world frame. $\{B\}$ is coincident with $\{W\}$ when all P joints are at their home position, as shown in Fig. 8. In the APPENDIX, the inverse kinematic model (IKM) of this robot is introduced, and a detailed constraint analysis of this robot is presented.

Suppose the feet of the hexapod robot with parallel legs are at the same level, and all the feet are anchored to six vertexes of an imaginary regular hexagon one-to-one. Fig. 9 shows the hexapod robot's workspace under the conditions mentioned above (by setting positions of all the feet and limits for all the joint variables, the workspace can be determined using the IKM). Each point in this figure represents a reachable position of the origin of $\{B\}$ while the orientation remains unchanged.

In order to investigate the effect of actuation patterns on the lowest power consumption, the indexes LNPC and MLNPC are used, which are associated with the lowest power consumption. According to the flowcharts shown in Figs. 6 and 7, if the configuration $\mathcal{C}$, the body twist $\mathcal{V}_b$, and the gravity force $\boldsymbol{f}_b$ are set, the LNPC and MLNPC are only determined by the host actuator number n_h. Therefore, the remainder of this section investigates the influence of n_h on the indexes LNPC and MLNPC.

The conditions used in the simulations of this section are listed in Table I. The population size and step tolerance are parameters for the genetic algorithm solver. Note that the host actuator number may be different in different simulations.

TABLE I: The simulation conditions of Section V-B

Parameter	Value
n_{min}	6
n_{max}	18
${}^W\boldsymbol{f}_b$	$[0, -700N, 0]^T$
$\mathcal{V}_b$	$[0,\ 0,\ 0,\ 0.01m/s,\ 0,\ 0]^T$
Support legs	All legs
Anchored feet	All feet
Population size	400
Step tolerance	1×10^{-9}

The LNPC corresponding to 6 and 18 host actuators over the workspace shown in Fig. 9 are calculated. The total weight of the robot body and the payload is represented in $\{W\}$ as ${}^W\boldsymbol{f}_b$, it is set to act at the origin of $\{B\}$. Nevertheless, this point of action can be set to other positions. The robot's body twist is set to be a translational velocity of $0.01m/s$ along $+\hat{X}_W$. Note that the simulations do not deal with the translation process. Instead, it is assumed that the body possesses a constant translational velocity at different positions in the workspace, while the body motion between different positions is ignored for simplicity. By setting a horizontal translational

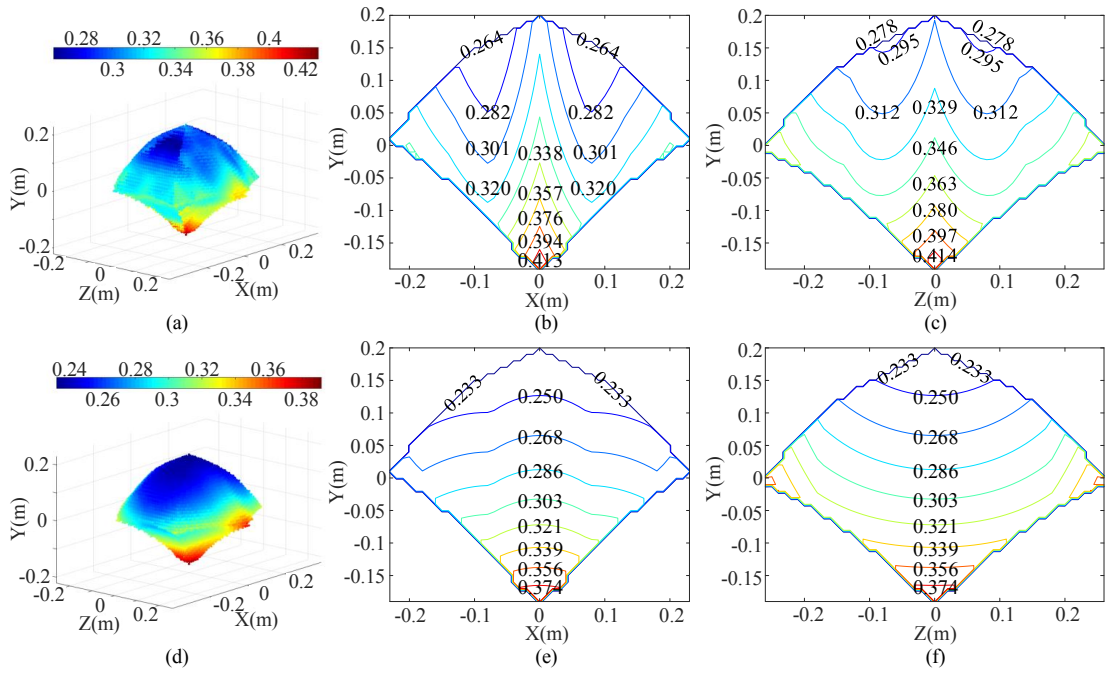

Fig. 10: The LNPC when the hexapod robot with parallel legs has a translational body velocity along $+\hat{X}_W$. The gravity acting on the body equals $700N$. (a)-(c) and (d)-(f) are the results corresponding to 6 and 18 host actuators respectively. (b) and (c) are the results on the $\hat{X}_W$-$\hat{Y}_W$ plane and $\hat{Y}_W$-$\hat{Z}_W$ plane of (a) respectively. (e) and (f) are the results on the $\hat{X}_W$-$\hat{Y}_W$ plane and $\hat{Y}_W$-$\hat{Z}_W$ plane of (d) respectively. The unit of the LNPC is $W \cdot N^{-1} \cdot (m/s)^{-1}$.

velocity direction such as $+\hat{X}_W$, it is easier to reveal the relationship between the LNPC and the host actuator number n_h according to other performed simulations. Nevertheless, other translational velocity directions can be adopted.

The calculation results are shown in Fig. 10. It can be found that the LNPC values at the bottom of the workspace are higher than the values at other parts. This phenomenon is understandable. Considering the hexapod robot's structure shown in Fig. 8, all the actuated prismatic joints are tilt upward and towards the body. When the body goes down, a host prismatic joint needs to increase output force to support the body since the component force along the vertical direction decreases. Thus, the power consumption at the bottom of the workspace is higher. However, in this figure, the LNPC relating to 6 host actuators is higher than 18 host actuators. This phenomenon is counterintuitive since fewer host actuators consumed more power in the simulation.

In order to explain the results shown in Fig. 10, the contributions of the mechanical power and the heat power to the LNPC are calculated separately. As shown in Fig. 11, the power consumption due to mechanical power is not zero, even though the robot body has a horizontal velocity (the robot's mechanical energy is not increasing). This phenomenon indicates the existence of *mechanical antagonism* [37], which describes the situation wherein the host actuators are working against each other. The electrical power dissipated by motors to work against each other is called *antagonistic power* in the literature. The mechanical antagonism is prevalent among legged robots [37], [13]. The mechanical power with regard to 6 host actuators, as shown in Fig. 11(a)-(b), is lower than that with regard to 18 host actuators, as shown in Fig. 11(c)-(d). On the other hand, the heat power relating to 6 host actuators, as shown in Fig. 12(a)-(b), is higher than that with regard to 18 host actuators, as shown in Fig. 12(c)-(d).

In order to verify whether or not the phenomenon revealed in Figs. 11 and 12 is general for the hexapod robot with parallel legs, simulations corresponding to 6 to 18 host actuators over the workspace are carried out. The index MLNPC is employed, which is less accurate than LNPC. However, using MLNPC makes it easier to inspect the power consumption corresponding to different host actuator numbers in the same figure. The simulation results are shown in Fig. 13. It can be found that, with the increase of the host actuator number n_h in the optimal actuation pattern, the power consumption due to mechanical power increases, whereas the power consumption due to heat decreases. This phenomenon is intuitive. In the case of mechanical power, engaging more host actuators increases the dimension of the antagonistic joint forces, which leads to the increase of the antagonistic power. Thus the power consumption due to mechanical power is increased. As for the heat power, more host actuators mean that the host joint force vector $\boldsymbol{\tau}_h$ with the minimal two-norm can be obtained from a higher-dimensional joint space according to Eq. 32 (Eq. 45 for the unanchored feet condition). Hence, the two-norm of the host joint force vector corresponding to the optimal actuation pattern decreases with the host actuator number, and thus an optimal actuation pattern with more host actuators generates a lower heat power according to the item $\frac{R_w}{k_t^2 G^2} \cdot \tau_g^2$ in Eq. 25.

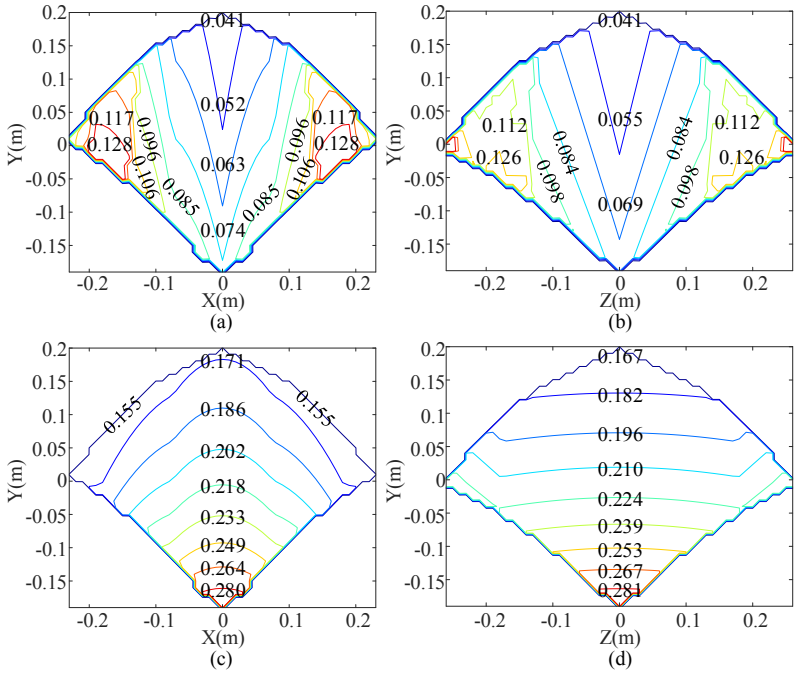

Fig. 11: The LNPC due to mechanical power when the hexapod robot with parallel legs has a translational body velocity along $+\hat{X}_W$. (a) and (b) are the results corresponding to 6 host actuators, (c) and (d) are the results corresponding to 18 host actuators. The gravity acting on the body is $700N$. The unit of the LNPC is $W \cdot N^{-1} \cdot (m/s)^{-1}$.

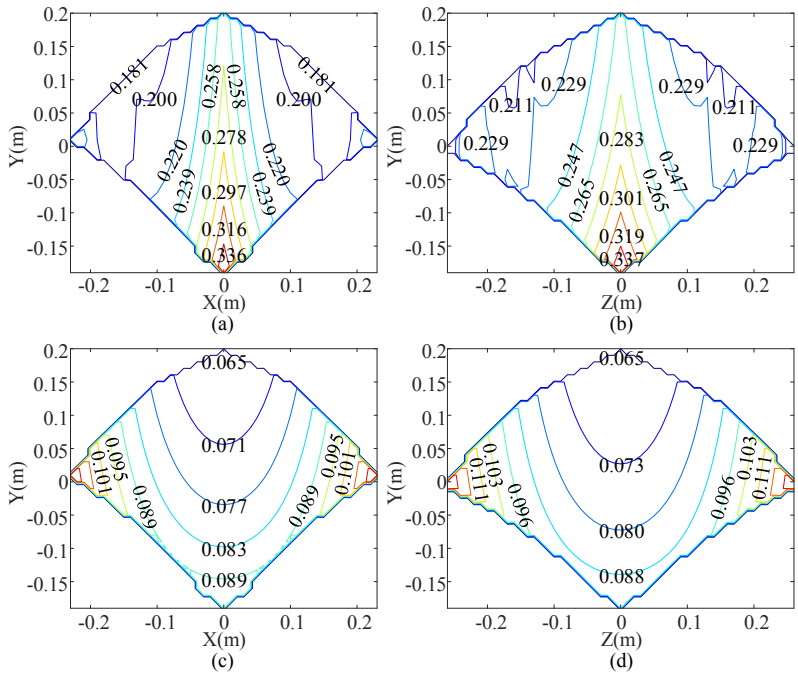

Fig. 12: The LNPC due to the heat power of resistance when the hexapod robot with parallel legs has a translational body velocity along $+\hat{X}_W$. (a) and (b) are the results corresponding to 6 host actuators, (c) and (d) are the results corresponding to 18 host actuators. The gravity acting on the body is $700N$. The unit of the LNPC is $W \cdot N^{-1} \cdot (m/s)^{-1}$.

C. Effect of actuation pattern on the average of the lowest power consumption of the hexapod robot with parallel legs under different payloads

According to Eq. 25, the mechanical power is affected by τ_g, while the heat power is influenced by τ_g^2. Moreover, the host joint force vector $\boldsymbol{\tau}_h$ is affected by the gravity force $\boldsymbol{f}_b$ (the payload). Therefore, it is necessary to study the power consumption under different $\boldsymbol{f}_b$. In this section, the lowest power consumption of the hexapod robot with parallel legs under different $\|\boldsymbol{f}_b\|$ is calculated.

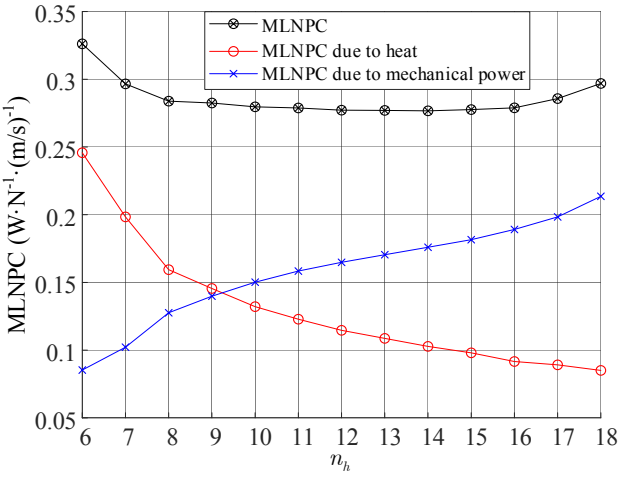

Fig. 13: The MLNPC when the hexapod robot with parallel legs has a translational body velocity along $+\hat{X}_W$. The gravity acting on the body is $700N$.

TABLE II: The simulation conditions of Section V-C

Parameter	Value
n_{min}	6
n_{max}	18
${}^W\boldsymbol{f}_b$	$[0, -\|\boldsymbol{f}_b\|, 0]^T$, $10N \leqslant \|\boldsymbol{f}_b\| \leqslant 3000N$
$\mathcal{V}_b$	$[0,\ 0,\ 0,\ 0.01m/s,\ 0,\ 0]^T$ $[0,\ 0,\ 0,\ 0,\ 0.01m/s,\ 0]^T$ $[0,\ 0,\ 0,\ 0,\ -0.01m/s,\ 0]^T$ $[0,\ 0,\ 0,\ 0,\ 0,\ 0.01m/s]^T$
Support legs	All legs
Anchored feet	All feet
Population size	400
Step tolerance	1×10^{-9}

The index MLNPC is used, which can represent the average of the lowest power consumption achieved by actuation patterns that have n_h host actuators. The MLNPC over the workspace shown in Fig. 9 with regard to different n_h is calculated. The robot body has a translational velocity along $+\hat{X}_W$, $+\hat{Y}_W$, $-\hat{Y}_W$, and $+\hat{Z}_W$ respectively in different simulations. For the reason of symmetry, the simulations corresponding to the body translational velocity along $-\hat{X}_W$ and $-\hat{Z}_W$ are omitted. The simulation conditions are listed in Table II.

Fig. 14 shows the MLNPC corresponding to the body translational velocity along $+\hat{X}_W$ and $+\hat{Z}_W$, respectively. The manner of the MLNPC changes with $\|\boldsymbol{f}_b\|$ can be explained as follows. Since a motor's heat power is proportional to τ_g^2 while a motor's mechanical power is proportional to τ_g, the change of the robot's heat power with $\|\boldsymbol{f}_b\|$ is one order higher than that of the robot's mechanical power with $\|\boldsymbol{f}_b\|$. When $\|\boldsymbol{f}_b\|$ is small, the MLNPC is dominated by the mechanical power. In this condition, the MLNPC can be reduced by choosing the actuation pattern with fewer host actuators since the antagonistic power and thus the mechanical power is reduced. However, when $\|\boldsymbol{f}_b\|$ is big, the MLNPC is dominated by the heat power. In this condition, the MLNPC can be reduced by choosing the actuation pattern with more host actuators since the electrical power dissipated as heat is reduced.

Fig. 15 is extracted from Fig. 14(a) to make the figure

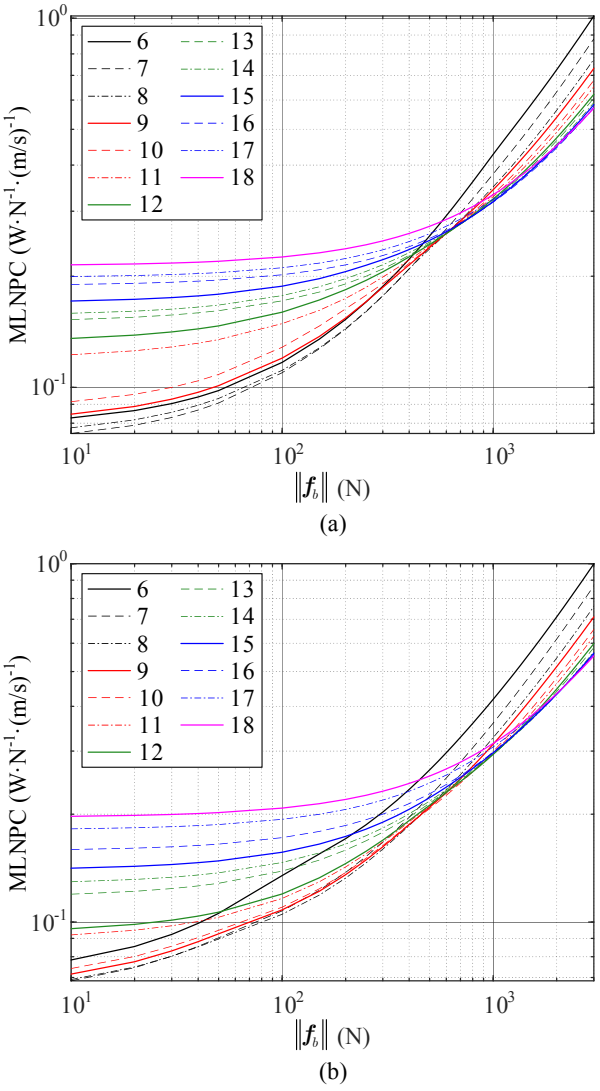

Fig. 14: The MLNPC when the hexapod robot with parallel legs has a translational body velocity along $+\hat{X}_W$ (a) and $+\hat{Z}_W$ (b) respectively. The gravity acting on the body varies from $10N$ to $3000N$. Numbers in the legend label the MLNPC with regard to different host actuator numbers.

uncluttered, which shows the curves of MLNPC corresponding to 6, 12, and 18 host actuators, respectively. As shown in this figure, when $\|\boldsymbol{f}_b\| \leqslant 420N$, the MLNPC relating to 6 host actuators is the lowest since the mechanical power dominates in this interval. When $\|\boldsymbol{f}_b\| \geqslant 1270N$, the MLNPC relating to 18 host actuators is the lowest since the heat power dominates in this interval. When $420N < \|\boldsymbol{f}_b\| < 1270N$, the MLNPC relating to 12 host actuators is the lowest. Moreover, when $\|\boldsymbol{f}_b\| \geqslant 570N$, the MLNPC relating to 18 host actuators is less than that relating to 6 host actuators, which is consistent with the results shown in Figs. 10 and 13.

Fig. 16 shows the MLNPC when the body of the hexapod robot with parallel legs has a translational velocity along $+\hat{Y}_W$ and $-\hat{Y}_W$. The curves shown in Fig. 16 are quite different from the curves shown in Fig. 14. As shown in Fig. 16(a), in this case, there is a negative correlation between the host actuator

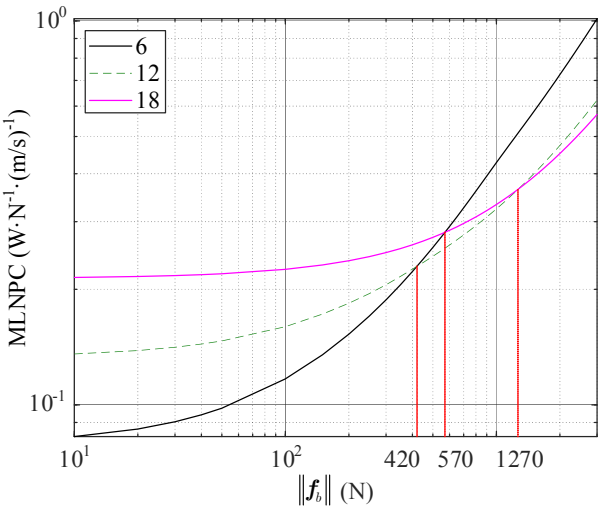

Fig. 15: The MLNPC when the hexapod robot with parallel legs has a translational body velocity along $+\hat{X}_W$ with 6, 12, and 18 host actuators respectively. The gravity acting on the body varies from $10N$ to $3000N$. Numbers in the legend label the MLNPC with regard to different host actuator numbers.

number and the MLNPC in the majority of the considered interval of $\|\boldsymbol{f}_b\|$. The clue to explain this phenomenon lies with the specific structure of the hexapod robot with parallel legs. As shown in Fig. 8, since all P joints are installed mainly in upward directions, the joint forces generated by them also point upwards. When the body translational velocity is along $+\hat{Y}_W$, the lengths of all the P joints increase. Thus, $\tau_g \cdot \dot{\theta}_g$ in Eq. 25 is positive, which means there is no antagonistic power. Therefore, by engaging more host actuators, lower power consumption can be acquired since the two-norm of the host joint force vector and thus the heat power is lower. The two cases shown in Fig. 16 are similar. The main difference is that there is no need to consume electrical power to elevate the body when it has a translational velocity along $-\hat{Y}_W$. In this case, all motors are working as dampers that dissipate the robot's potential energy. However, the host actuators still need to support the payload. Thus the heat power still exits.

D. Effect of the actuation pattern on the lowest power consumption of legged robots considering general conditions

Sections V-B and V-C studied the effect of actuation patterns on the lowest power consumption of the hexapod robot with parallel legs under conditions that the body has translational velocities, and the feet are anchored on the ground. This section performs numerical experiments to check whether the effect of actuation patterns on the lowest power consumption maintains unchanged considering the general motion, the unanchored feet condition, and a more general robot structure.

1) Numerical experiments of the hexapod robot with parallel legs performs general body motion: A multi-dimensional helical path $q(\sigma), \sigma \in [0, 1]$ of the body frame $\{B\}$ is designed as an example of a general path, which is shown in Fig. 17. $q(\sigma)$ maps the scalar parameter σ to the pose of $\{B\}$. When following this path, the $\hat{Y}_B$-axis always tilts towards the axis

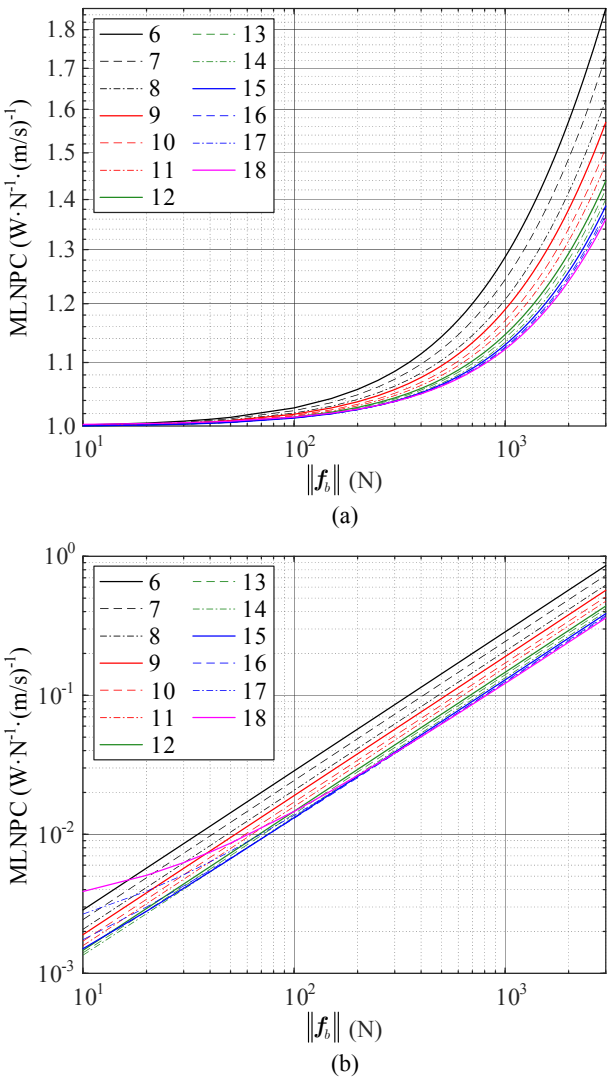

Fig. 16: The MLNPC when the hexapod robot with parallel legs has a translational body velocity along $+\hat{Y}_W$ (a) and $-\hat{Y}_W$ (b) respectively. The gravity acting on the body varies from $10N$ to $3000N$. Numbers in the legend label the MLNPC with regard to different host actuator numbers.

TABLE III: The simulation conditions of Section V-D1

Parameter	Value
n_h	6, 12, 18
${}^W\boldsymbol{f}_b$	$[0, -\|\boldsymbol{f}_b\|, 0]^T, \|\boldsymbol{f}_b\| = 10, 100, 1000, 3000N$
$\|\mathcal{V}_b\|$	$0.01m/s$
Support legs	All legs
Anchored feet	All feet
Population size	400
Step tolerance	1×10^{-9}

of the path (as shown in Fig. 17). Thus the body changes its position and orientation during the motion.

Numerical experiments of the hexapod robot with parallel legs manipulates its body along the helical path are carried out. The simulation conditions are listed in Table III. Fig. 18 shows the LNPC obtained in these numerical experiments.

2) Numerical experiments of the hexapod robot with serial legs moves its body under the unanchored feet condition: Fig.

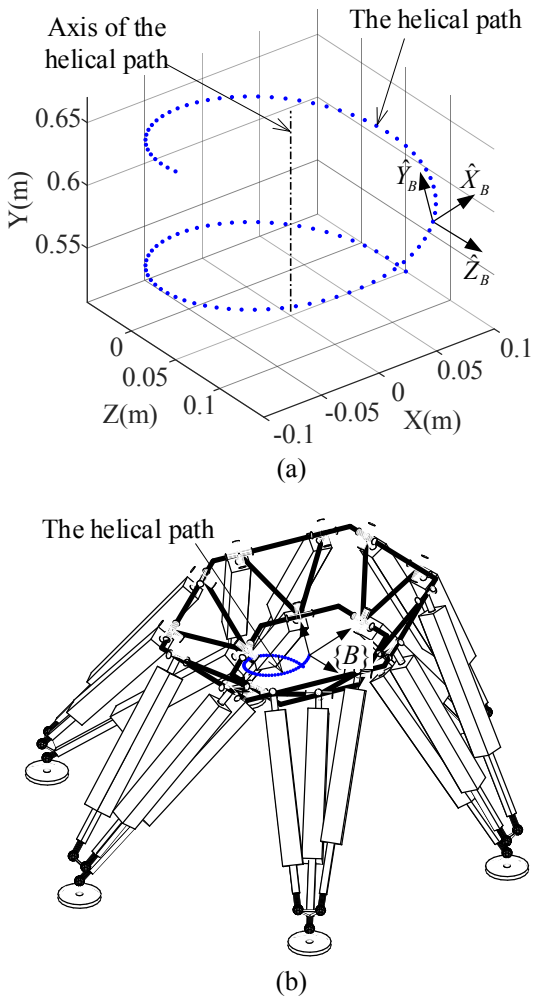

Fig. 17: The body of the hexapod robot with parallel legs moves along a helical path. (a) The helical path. (b) A snapshot of the motion.

19(a) shows the legged robot employed in this section. This robot has six identical legs. Each leg is a RRR (revolute joint - revolute joint - revolute joint) serial mechanism with a ball-shaped foot at the end, as shown in Fig. 19(b). All the R joints are actuated. The body frame $\{B\}$ is attached to the center of the body. $\{W\}$ is the world frame.

TABLE IV: The simulation conditions of Section V-D2

Parameter	Value
n_h	7, 8, 9
${}^W\boldsymbol{f}_b$	$[0, -\|\boldsymbol{f}_b\|, 0]^T$, $\|\boldsymbol{f}_b\| = 10, 100, 1000, 3000N$
$\mathcal{V}_b$	$[0,\ 0,\ 0,\ 0,\ 0,\ 0.01m/s]^T$
μ	1
Support legs	leg_1, leg_3, and leg_5
Swing legs	leg_2, leg_4, and leg_6
Anchored feet	None
Population size	400
Step tolerance	1×10^{-9}

Suppose the legged robot uses the tripod gait to walk. Fig. 19(a) shows the beginning of a walking phase. During this walking phase, the support feet are at the same level; the body translates along a straight-line path, which is coincident with

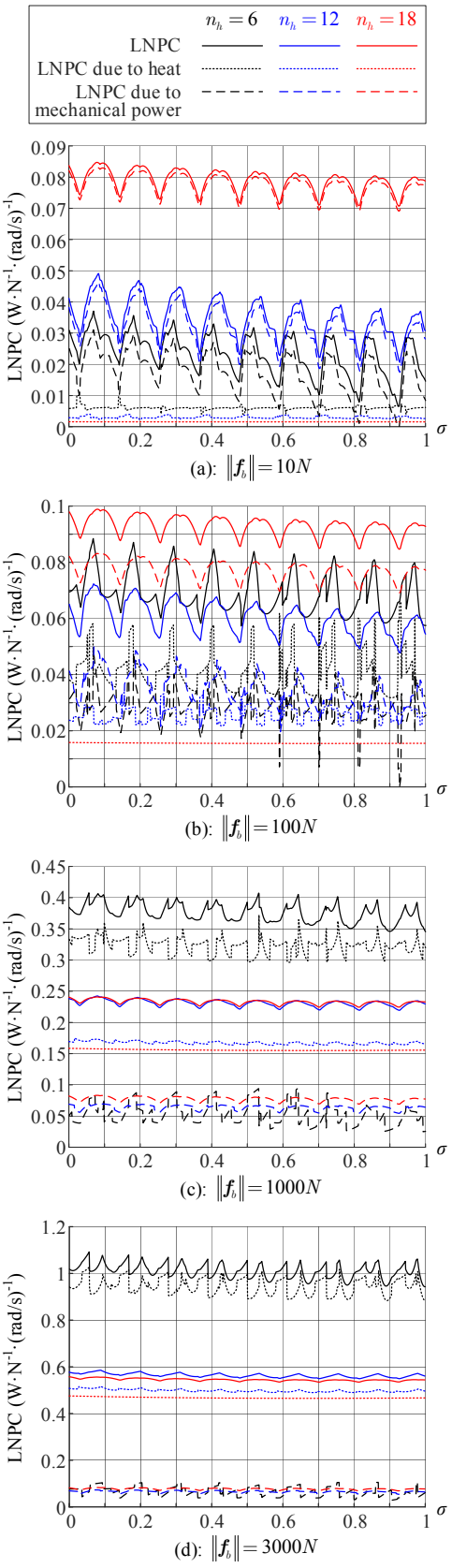

Fig. 18: The LNPC when the body of the hexapod robot with parallel legs moves along a helical path.

the $\hat{Z}_W$-axis and is symmetrically divided by the $\hat{X}_W$-$\hat{Y}_W$ plane, as shown in Fig. 19(c). During the translation, $\{B\}$ is aligned with $\{W\}$. Moreover, when $\{B\}$ is coincident with $\{W\}$, all the support legs possess the same posture.

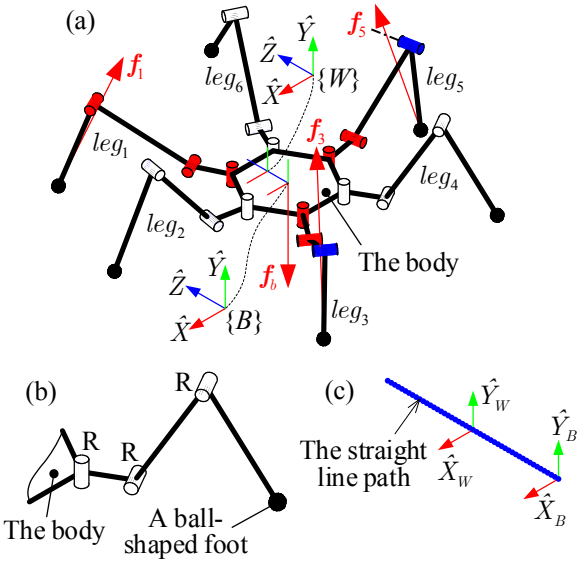

Fig. 19: The body of the hexapod robot with serial legs moves along a straight line path during a walking phase. (a) The hexapod robot at the beginning of the walking phase. This figure shows that there are seven host joints in the actuation pattern corresponding to this instant. The host joints are drawn in red, the slave joints are drawn in blue, and the swing legs' joints are drawn in white. (b) The structure of the serial leg. (c) The straight line path.

Numerical experiments about the walking phase mentioned above are performed. The simulation conditions are listed in Table IV. μ is the static coefficient of friction between the support feet and the ground. In Fig. 19(a), the contact forces are depicted, which are obtained by solving the optimization problem defined in Eq. 47. As shown in this figure, $\boldsymbol{f}_3$ and $\boldsymbol{f}_5$ intersect the axis of the corresponding slave joint. Thus, $\boldsymbol{f}_3$ and $\boldsymbol{f}_5$ cannot cause reactive force in the corresponding slave joint. This result is obtained by introducing the constraint condition relating to the actuation pattern shown in Eq. 47. Fig. 20 shows the LNPC obtained in these numerical experiments.

3) Discussion: It can be found from Figs. 18 and 20 that: a) under the condition of the same $\|\boldsymbol{f}_b\|$, the mechanical power increases with n_h, whereas the heat power decreases with n_h; b) under the condition of the same n_h, the proportion of mechanical power to the total power decreases with $\|\boldsymbol{f}_b\|$, whereas the proportion of heat power to the total power increases with $\|\boldsymbol{f}_b\|$; c) the mechanical power dominates the power consumption when $\|\boldsymbol{f}_b\|$ is small, whereas the heat power dominates the power consumption when $\|\boldsymbol{f}_b\|$ is big. The explanations for these results are similar to that given in Sections V-B and V-C and are omitted here. These results indicate that the effect of actuation patterns on the lowest power consumption of legged robots maintains unchanged considering the general motion, different structures, and the feet anchoring state.

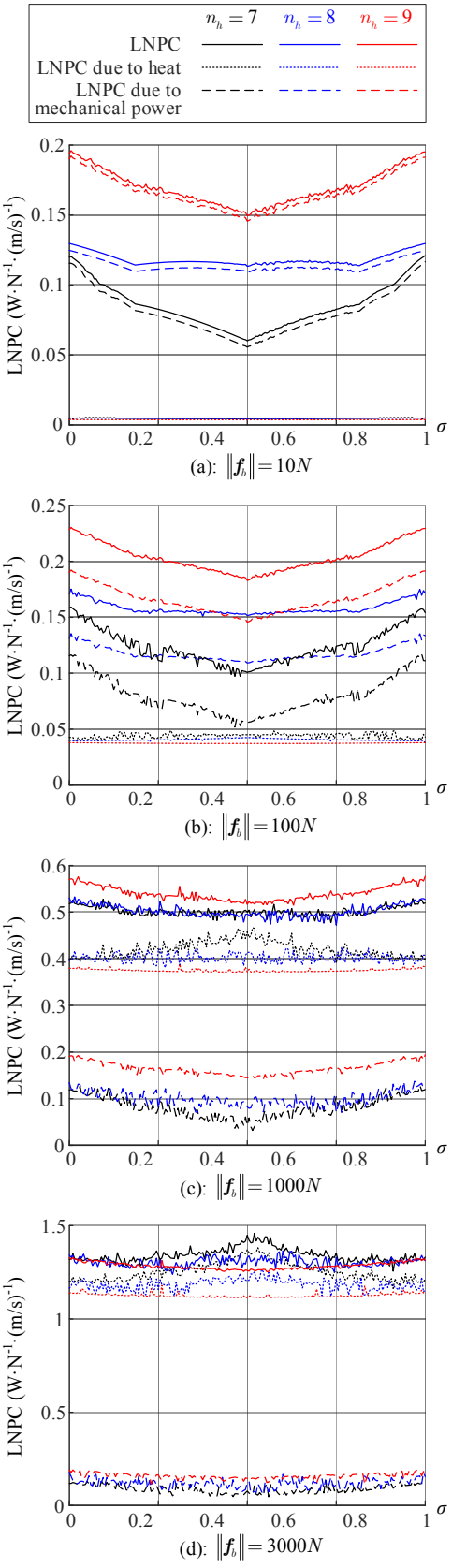

Fig. 20: The LNPC when the body of the hexapod robot with serial legs moves along a straight line path.

VI. Conclusions

This article investigated the effect of actuation patterns on the power consumption of legged robots that work in a quasi-static manner. First, the effect of actuation patterns on the power consumption of the hexapod robot with parallel legs is investigated through numerical experiments wherein the feet are anchored on the ground, and the body has translational velocities. Second, numerical experiments are carried out to check whether the aforementioned effect of actuation patterns maintains unchanged considering the general motion, the unanchored feet condition, and a more general legged robot. The obtained results can be concluded as follows:

- Increasing the host actuator number in the optimal actuation pattern can reduce the power consumption due to heat power whereas increase the power consumption due to mechanical power;
- The proportion of the mechanical power to the total power decreases with the payload, whereas the proportion of the heat power to the total power increases with the payload;
- The mechanical power dominates the total power when the payload is small, whereas the heat power dominates the total power when the payload is big.

These results indicate that a legged robot's total power consumption can be reduced by choosing actuation patterns properly. More specifically, a legged robot's total power consumption can be reduced by choosing actuation patterns with fewer host actuators when the payload is small and by choosing actuation patterns with more host actuators when the payload is big. This approach provided a new option for the motion planning of legged robots in terms of minimization of power consumption.

The work reported above is a theoretical result. To make it applicable, the next work will be to develop a corresponding actuation pattern planning method to determine the actuation pattern series for an energy-efficient motion. When all the other factors are the same, the optimal actuation pattern is determined by the specific configuration and body twist of the legged robot. When performing general tasks, these two factors and thus the optimal actuation pattern changes. Therefore, it is impractical to drive a legged robot with the optimal actuation pattern corresponding to each specific configuration and body twist, since it is impractical to switch the driving state of an actuator continuously. A solution to this problem is to divide a motion task into sub-tasks and choose the optimal actuation pattern for each sub-task. In this way, the power consumption will be higher than that of the driving scheme that always adopts optimal actuation patterns. Obtaining a practical driving scheme for a legged robot with the conclusions of this article will be the theme of a future study.

Appendix

A. The inverse kinematic model of the hexapod robot with parallel legs

For the hexapod robot with parallel legs, the inverse kinematic model (IKM) calculates the joint coordinates from the pose of the body and positions of all feet. The IKM can be represented as follows:

$$(\boldsymbol{\theta}_r, \boldsymbol{\Theta}) = \mathrm{IKM}({}^W_B T, {}^W\mathrm{S}_{f_1}, {}^W\mathrm{S}_{f_2}, {}^W\mathrm{S}_{f_3}, {}^W\mathrm{S}_{f_4}, {}^W\mathrm{S}_{f_5}, {}^W\mathrm{S}_{f_6}), \tag{49}$$

where $\boldsymbol{\theta}_r = [\theta_1, \theta_2, \cdots, \theta_{18}]^T$ is the joint variable vector of P joints, each element of $\boldsymbol{\theta}_r$ represents the length of one prismatic joint; $\boldsymbol{\Theta}$ is the joint variable vector of all the passive joints; ${}^W_B T$ represents pose of body frame $\{B\}$ relative to world frame $\{W\}$; ${}^W\mathrm{S}_{f_1}$, ${}^W\mathrm{S}_{f_2}$, ${}^W\mathrm{S}_{f_3}$, ${}^W\mathrm{S}_{f_4}$, ${}^W\mathrm{S}_{f_5}$, and ${}^W\mathrm{S}_{f_6}$ represent positions of all the feet relative to $\{W\}$; ${}^W_B T$, ${}^W\mathrm{S}_{f_1}$, ${}^W\mathrm{S}_{f_2}$, ${}^W\mathrm{S}_{f_3}$, ${}^W\mathrm{S}_{f_4}$, ${}^W\mathrm{S}_{f_5}$, and ${}^W\mathrm{S}_{f_6}$ can be retrieved from the hexapod robot's configuration $\mathcal{C}$. The detailed derivation process of the IKM can be found in [38].

B. The constraint analysis of the hexapod robot with parallel legs

The constraint analysis is required for determining feasible actuation patterns. This section presents the constraint analysis of the hexapod robot with parallel legs.

Since the hexapod robot and the ground can be treated as an equivalent parallel robot, the body constraint-screw system is the union of all the leg constraint-screw systems. Thus, the remainder of this section analyzes the leg constraint-screw system.

Since each leg is a hybrid mechanism, which consists of a 1UP-2UPS parallel mechanism and a serially connected spherical joint, the constraint analysis of the leg is divided into two parts. The constraints generated by the 1UP-2UPS mechanism corresponding to different actuation patterns are analyzed firstly. The leg constraint-screw system can be obtained afterward.

For convenience, the UP branch is referred to as branch 1, and the two UPS branches are referred to as branch 2 and branch 3, respectively. Fig. 21 shows the joint screws and constraint screws of the 1UP-2UPS mechanism's branches. The determining of joint screws is an inverse kinematics problem, which can be solved with the results of Eq. 49.

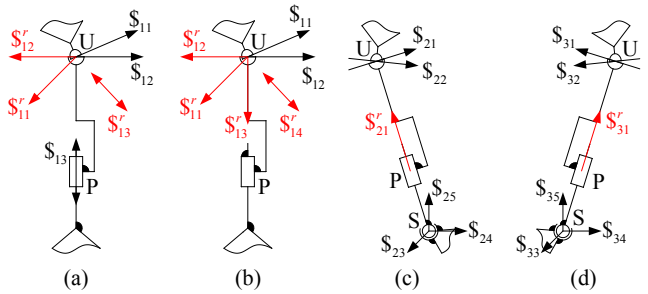

Fig. 21: Joint and constraint screws of the branches of the 1UP-2UPS mechanism. The joint screws are drawn in black and the constraint screws in red. Line vectors are plotted as arrows. Couples are plotted as double-headed arrows. The first digit in the subscript of each item indicates the branch. (a) Branch 1 with a slave joint (UP branch). (b) Branch 1 with a host joint. (c) Branch 2 with a host joint (UPS branch). (d) Branch 3 with a host joint (UPS branch).

In the case of the UP branch, when the P joint is a slave joint, the motion-screw system of this branch is:

$$\mathbb{S}_1 = [\$_{11}, \$_{12}, \$_{13}], \tag{50}$$

where $\$_{11}$ and $\$_{12}$ are the joint screws of the U joint, and $\$_{13}$ is the joint screw of the P joint, as shown in Fig. 21 (a). The corresponding constraint-screw system can be deduced as:

$$\mathbb{S}_1^r = \Delta\mathbb{N}(\mathbb{S}_1^T) = [\$_{11}^r, \$_{12}^r, \$_{13}^r], \tag{51}$$

where $\mathbb{N}(\mathbb{S}_1^T)$ is the null space of the transpose of $\mathbb{S}_1$. When the P joint is a host joint, it can be treated as a locked joint. Thus the motion-screw system of the UP branch becomes:

$$\mathbb{S}_1 = [\$_{11}, \$_{12}]. \tag{52}$$

Accordingly, the constraint-screw system becomes:

$$\mathbb{S}_1^r = \Delta\mathbb{N}(\mathbb{S}_1^T) = [\$_{11}^r, \$_{12}^r, \$_{13}^r, \$_{14}^r], \tag{53}$$

as shown in Fig. 21 (b).

In the case of branch 2, when the P joint is a host joint, the motion-screw system is:

$$\mathbb{S}_2 = [\$_{21}, \$_{22}, \$_{23}, \$_{24}, \$_{25}], \tag{54}$$

where $\$_{21}$ and $\$_{22}$ are the joint screws of the U joint, and $\$_{23}$, $\$_{24}$, and $\$_{25}$ are the joint screws of the S joint. The corresponding constraint-screw system can be deduced as:

$$\mathbb{S}_2^r = \Delta\mathbb{N}(\mathbb{S}_2^T) = \$_{21}^r, \tag{55}$$

as shown in Fig. 21 (c). When the P joint is a slave joint, this branch can not generate any constraints. The analysis of branch 3 is the same as that of branch 2. The motion-screw system $\mathbb{S}_3$ and the corresponding constraint-screw system $\mathbb{S}_3^r$ are shown in Fig. 21 (d).

The constraint-screw system $\mathbb{S}_{up}^r$ of the 1UP-2UPS mechanism is the union of all the branches' constraint-screw systems:

$$\mathbb{S}_{up}^r = \mathbb{S}_1^r \cup \mathbb{S}_2^r \cup \mathbb{S}_3^r. \tag{56}$$

Table V shows the $\mathbb{S}_{up}^r$ relating to different actuation patterns.

TABLE V: The constraint-screw systems $\mathbb{S}_{up}^r$ of the 1UP-2UPS mechanism. P_1, P_2, and P_3 represent the P joint in branch 1, branch 2, and branch 3 respectively. '0' represents the slave state and '1' represents the host state.

	Actuation pattern			$\mathbb{S}_{up}^r$
	P_1	P_2	P_3	
Case 1	0	0	0	$\varnothing$
Case 2	1	0	0	$[\$_{11}^r, \$_{12}^r, \$_{13}^r, \$_{14}^r]$
Case 3	0	1	0	$\$_{21}^r$
Case 4	0	0	1	$\$_{31}^r$
Case 5	1	1	0	$[\$_{11}^r, \$_{12}^r, \$_{13}^r, \$_{14}^r, \$_{21}^r]$
Case 6	1	0	1	$[\$_{11}^r, \$_{12}^r, \$_{13}^r, \$_{14}^r, \$_{31}^r]$
Case 7	0	1	1	$[\$_{21}^r, \$_{31}^r]$
Case 8	1	1	1	$[\$_{11}^r, \$_{12}^r, \$_{13}^r, \$_{14}^r, \$_{21}^r, \$_{31}^r]$

The 1UP-2UPS mechanism can be treated as a compound joint, its joint screw system is:

$$\mathbb{S}_{up} = \Delta\mathbb{N}([\mathbb{S}_{up}^r]^T). \tag{57}$$

The leg constraint-screw system can be deduced from the leg motion-screw system base on the reciprocity between motion and constraint. Since the leg is constructed by connecting the 1UP-2UPS mechanism and a spherical joint in serial, the leg motion is simply the union of the motion of these two parts. Hence, the following relation exists:

$$\mathbb{S}_l = \mathbb{S}_{up} \cup \mathbb{S}_f, \tag{58}$$

where $\mathbb{S}_l$ is the leg motion screw system, and $\mathbb{S}_f$ is the joint screw system of the spherical joint S_f at the end of the leg.

$$\mathbb{S}_f = [\$_{f_1}, \$_{f_2}, \$_{f_3}], \tag{59}$$

where $\$_{f_1}$, $\$_{f_2}$, and $\$_{f_3}$ are line vectors that passing through the joint S_f and linearly independent with each other.

Now the leg constraint-screw system $\mathbb{S}_l^r$ can be deduced as:

$$\mathbb{S}_l^r = \Delta\mathbb{N}(\mathbb{S}_l^T). \tag{60}$$

REFERENCES

[1] K. H. Williford, K. A. Farley, K. M. Stack, A. C. Allwood, D. Beaty, L. W. Beegle, R. Bhartia, A. J. Brown, M. de la Torre Juarez, S.-E. Hamran, M. H. Hecht, J. A. Hurowitz, J. A. Rodriguez-Manfredi, S. Maurice, S. Milkovich, and R. C. Wiens, "Chapter 11 - the nasa mars 2020 rover mission and the search for extraterrestrial life," in *From Habitability to Life on Mars*. Elsevier, 2018, pp. 275–308.

[2] T. Zhang, K. Xu, Z. Yao, X. Ding, Z. Zhao, X. Hou, Y. Pang, X. Lai, W. Zhang, S. Liu *et al.*, "The progress of extraterrestrial regolith-sampling robots," *Nature Astronomy*, vol. 3, no. 6, pp. 487–497, 2019.

[3] S. Bartsch, T. Birnschein, M. Römmermann, J. Hilljegerdes, D. Kühn, and F. Kirchner, "Development of the six-legged walking and climbing robot spaceclimber," *Journal of Field Robotics*, vol. 29, no. 3, pp. 506–532, 2012.

[4] P. Arm, R. Zenkl, P. Barton, L. Beglinger, A. Dietsche, L. Ferrazzini, E. Hampp, J. Hinder, C. Huber, D. Schaufelberger, F. Schmitt, B. Sun, B. Stolz, H. Kolvenbach, and M. Hutter, "Spacebok: A dynamic legged robot for space exploration," in *2019 International Conference on Robotics and Automation (ICRA)*, Montreal, Canada, May 2019, pp. 6288–6294.

[5] A. Parness, N. Abcouwer, C. Fuller, N. Wiltsie, J. Nash, and B. Kennedy, "Lemur 3: A limbed climbing robot for extreme terrain mobility in space," in *2017 IEEE International Conference on Robotics and Automation (ICRA)*, Singapore, May 2017, pp. 5467–5473.

[6] B. H. Wilcox, "Athlete: A limbed vehicle for solar system exploration," in *2012 IEEE Aerospace Conference*, Big Sky, MT, USA, Mar 2012, pp. 1–9.

[7] R. Lin, W. Guo, and M. Li, "Novel design of legged mobile landers with decoupled landing and walking functions containing a rhombus joint," *Journal of Mechanisms and Robotics*, vol. 10, no. 6, p. 061017, 2018.

[8] B. V. Oaida, K. Lewis, E. Ferguson, J. Day, and K. McCoy, "A statistical approach to payload energy management for nasa's europa clipper mission," in *2018 IEEE Aerospace Conference*, Big Sky, MT, USA, Mar 2018, pp. 1–12.

[9] C. Li, Z. Wei, W. Wen, X. Zeng, X. Gao, Y. Liu, Q. Fu, Z. Zhang, Y. Su, X. Ren, F. Wang, J. Liu, W. Yan, X. Tan, D. Liu, B. Liu, H. Zhang, and Z. Ouyang, "Overview of the chang'e-4 mission: Opening the frontier of scientific exploration of the lunar far side," *Space Science Reviews*, vol. 217, no. 35, pp. 1–35, 2021.

[10] J. Yang, W. Jia, Y. Sun, H. Pu, S. Ma, L. Chen, and Bin Han, "Mechanical design of a compact and dexterous quadruped robot," in *2017 IEEE International Conference on Mechatronics and Automation (ICMA)*, Takamatsu, JAPAN, Aug 2017, pp. 1450–1456.

[11] A. Mazumdar, S. J. Spencer, C. Hobart, J. Dabling, T. Blada, K. Dullea, M. Kuehl, and S. P. Buerger, "Synthetic fiber capstan drives for highly efficient, torque controlled, robotic applications," *IEEE Robotics and Automation Letters*, vol. 2, no. 2, pp. 554–561, 2017.

[12] T. Zielinska, "Minimizing energy cost in multi-legged walking machines," *Journal of Intelligent & Robotic Systems*, vol. 85, no. 3, pp. 431–447, 2017.

[13] K. Koutsoukis and E. Papadopoulos, "On the effect of robotic leg design on energy efficiency," in *2021 IEEE International Conference on Robotics and Automation (ICRA)*, Xi'an, China, May 2021, pp. 9905–9911.

[14] M. Y. Harper, J. V. Nicholson, E. G. Collins, J. Pusey, and J. E. Clark, "Energy efficient navigation for running legged robots," in *2019 International Conference on Robotics and Automation (ICRA)*, Montreal, Canada, May 2019, pp. 6770–6776.

[15] A. Bodrov, W. Cheah, P. N. Green, S. Watson, and J. Apsley, "Joint space reference trajectory to reduce the energy consumption of a six-legged mobile robot," in *2018 25th International Workshop on Electric Drives: Optimization in Control of Electric Drives (IWED)*, Moscow, Russia, Jan 2018, pp. 1–6.

[16] H. Gao, Y. Liu, L. Ding, G. Liu, Z. Deng, Y. Liu, and H. Yu, "Low impact force and energy consumption motion planning for hexapod robot with passive compliant ankles," *Journal of Intelligent & Robotic Systems*, vol. 94, no. 2, pp. 349–370, 2019.

[17] H. Zhou, X. Feng, C. Ding, Z. Dong, C. Liu, Y. Zhang, and Z. Meng, "Yutu-2 radar sounding evidence of a buried crater at chang'e-4 landing site," *IEEE Transactions on Geoscience and Remote Sensing*, vol. 60, pp. 1–19, 2022.

[18] Y. Hu and W. Guo, "A new concept of contact joint to model the geometric foot-environment contacts for efficiently determining possible stances for legged robots," *Mechanism and Machine Theory*, vol. 162, p. 104327, 2021.

[19] C. Zhang, X. Wang, X. Wang, and J. S. Dai, "Modeling for a metamorphic quadruped robot with a twisting trunk: Kinematic and workspace," in *IECON 2017 - 43rd Annual Conference of the IEEE Industrial Electronics Society*, Beijing, China, 2017, pp. 6886–6892.

[20] A. Parness, A. Willig, A. Berg, M. Shekels, V. Arutyunov, C. Dandino, and B. Kennedy, "A microspine tool: Grabbing and anchoring to boulders on the asteroid redirect mission," in *2017 IEEE Aerospace Conference*, Big Sky, MT, USA, Mar 2017, pp. 1–10.

[21] S. Park, J. Kim, and G. Lee, "Optimal trajectory planning considering optimal torque distribution of redundantly actuated parallel mechanism," *Proceedings of the Institution of Mechanical Engineers, Part C: Journal of Mechanical Engineering Science*, vol. 232, no. 23, pp. 4410–4419, 2018.

[22] G. Lee, S. Park, D. Lee, F. C. Park, J. I. Jeong, and J. Kim, "Minimizing energy consumption of parallel mechanisms via redundant actuation," *IEEE/ASME Transactions on Mechatronics*, vol. 20, no. 6, pp. 2805–2812, 2015.

[23] J. Lee, G. Lee, and Y. Oh, "Energy-efficient robotic leg design using redundantly actuated parallel mechanism," in *2017 IEEE International Conference on Advanced Intelligent Mechatronics (AIM)*, Munich, Germany, Jul 2017, pp. 1203–1208.

[24] J. S. Dai and J. Sun, "Geometrical revelation of correlated characteristics of the ray and axis order of the plücker coordinates in line geometry," *Mechanism and Machine Theory*, vol. 153, p. 103983, 2020.

[25] H. Lipkin and J. Duffy, "The elliptic polarity of screws," *Journal of Mechanisms, Transmissions, and Automation in Design*, vol. 107, no. 3, pp. 377–386, 09 1985.

[26] R. S. Ball, "The theory of screws: A study in the dynamics of a rigid body," *Mathematische Annalen*, vol. 9, no. 4, pp. 541–553, 1876.

[27] J. S. Dai, Z. Huang, and H. Lipkin, "Mobility of overconstrained parallel mechanisms," *Journal of Mechanical Design*, vol. 128, no. 1, pp. 220–229, 10 2006.

[28] J. S. Dai and J. R. Jones, "Null-space construction using cofactors from a screw-algebra context," *Proceedings of the Royal Society of London. Series A: Mathematical, Physical and Engineering Sciences*, vol. 458, no. 2024, pp. 1845–1866, 2002.

[29] S. Bruno, S. Lorenzo, V. Luigi, and O. Giuseppe, *Robotics: Modelling, Planning and Control*. London: Springer, 2009, ch. Kinematics, pp. 39–103.

[30] K. Lynch and F. Park, *Modern Robotics*. Cambridge University Press, 2017.

[31] S. S. Roy and D. K. Pratihar, "Effects of turning gait parameters on energy consumption and stability of a six-legged walking robot," *Robotics and Autonomous Systems*, vol. 60, no. 1, pp. 72–82, 2012.

[32] H. Taghirad, *Parallel Robots: Mechanics and Control*. CRC Press, 2013, ch. Motion Control, pp. 303–316.

[33] X. Lin, J. Zhang, J. Shen, G. Fernandez, and D. W. Hong, "Optimization based motion planning for multi-limbed vertical climbing robots," in *2019 IEEE/RSJ International Conference on Intelligent Robots and Systems (IROS)*, Macau, China, Nov 2019, pp. 1918–1925.

[34] G. Wang, L. Ding, H. Gao, Z. Deng, Z. Liu, and H. Yu, "Minimizing the energy consumption for a hexapod robot based on optimal force distribution," *IEEE Access*, vol. 8, pp. 5393–5406, 2020.

[35] V. R. Kumar and K. J. Waldron, "Force distribution in closed kinematic chains," *IEEE Journal on Robotics and Automation*, vol. 4, no. 6, pp. 657–664, 1988.

[36] S. S. Roy and D. K. Pratihar, "Kinematics, dynamics and power consumption analyses for turning motion of a six-legged robot," *J. Intell. Robotics Syst.*, vol. 74, no. 3–4, p. 663–688, 2014.

[37] A. Abate, J. W. Hurst, and R. L. Hatton, "Mechanical antagonism in legged robots," in *Robotics: Science and Systems*, vol. 6, Ann Arbor, Michigan, USA, Jun 2016, pp. 1–8.

[38] Y. Pan and F. Gao, "Kinematic performance analysis for hexapod mobile robot using parallel mechanism," in *ASME 2014 International Design Engineering Technical Conferences and Computers and Information in Engineering Conference*, Buffalo, New York, USA, Aug 2014, p. V05AT08A089.

Yuan Hu received the Ph.D. degree in mechanical engineering from Shanghai Jiao Tong University, Shanghai, China, in 2021.

He is currently an instructor with the School of Mechanical Engineering, University of Shanghai for Science and Technology, Shanghai, China. His research interests include parallel mechanisms and legged robots.

Weizhong Guo received the Bachelor's degree in mechanical engineering from Ocean University of Qingdao, Qingdao, China, in 1993, the Master's degree in mechanical engineering from South-East University, Nanjing, China, in 1996, and the Ph.D. degree in mechanical engineering from Shanghai Jiao Tong University, Shanghai, China, in 1999.

He worked as a Postdoctoral Research Associate with the Department of Automation and Computer Aided Engineering, the Chinese University of Hong Kong, Hong Kong, China, from December 2001 to May 2002 and from January 2003 to July 2003. He acted as a Visiting Professor with University of Genova, Genova, Italy, Warsaw University of Technology, Warsaw, Poland, and Ecole Centrale de Nantes, Nantes, France, respectively. He is now a Full Professor with Tenure at Shanghai Jiao Tong University, Shanghai, China. His research focuses on parallel kinematic mechanisms and applications, mechanism analysis and synthesis, and innovation design of robotic systems. He co-authored 3 books, published several book chapters, more than 100 journal papers and conference papers, and holds more than 50 patents.

Prof. Guo is a senior member of CMES, a member of ASME, and a member of Permanent Commission for Education, IFToMM. He served as an Associate Editor of CEB for the IEEE ICRA in 2014 and 2015, and now serves as an Associate Editor of Mechanism and Machine Theory, as well as Machine Design & Research.

Rongfu Lin received the Ph.D. degree in mechanical engineering from Shanghai Jiao Tong University, Shanghai, China, in 2018.

He is currently a post-doctor at Shanghai Jiao Tong University. His research interests include parallel mechanisms and biomimetic robots. He is the author of more than 10 articles and 20 inventions.